Kinetics and Catalysis, Vol. 46, No. 4, 2005, pp. 578–596. Translated from Kinetika i Kataliz, Vol. 46, No. 4, 2005, pp. 615–634.

Nitrogen-Containing Paramagnetic Centers in Vitreous Silica

V. A. Radtsig

Semenov Institute of Chemical Physics, Russian Academy of Sciences, Moscow, 119991 Russia

Received December 10, 2003

Abstract—The results of a study on the structure and spectral characteristics of nitrogen-containing paramagnetic defects in vitreous silicas are presented. The UV irradiation, γ-irradiation, and mechanical destruction of nitrogen-doped vitreous silicas, which were synthesized using a plasma-chemical SPCVD technology, were used for the generation of paramagnetic centers. Another technique for producing nitrogen-containing paramagnetic centers was the target-oriented chemical modification of the surface defects of silica with the use of NH_3 (ND_3) molecules. Paramagnetic centers with free valences at silicon [$(\equiv Si–O–)_2Si^{\bullet}(–NH_2)$ and $(\equiv Si–O–)_2Si^{\bullet}–N(–Si\equiv)_2$] and nitrogen atoms [$\equiv Si–N^{\bullet}–H$ and $\equiv Si–N^{\bullet}–Si\equiv$] were detected. The reactivity of nitrogen-centered radicals toward H_2 and CO molecules was studied. Quantum-chemical calculations of model systems were employed in the interpretation of the experimental data. The strengths of Si–O and Si–N bonds in vitreous silica were compared.

INTRODUCTION

Nitrogen-doped vitreous silica exhibits a number of properties useful for potential practical applications [1, 2]. It is believed that amorphous silicon oxynitride can replace SiO_2 as a gate dielectric in a new generation of nanoscaled MOS devices [3]. Nitrogen-doped vitreous silicas can be used in fiber-optic devices and integrated optics [4]; these fibers exhibit enhanced photorefractivity and radiation stability [5, 6]. The effect of nitrogen dopant atoms on the spectral characteristics and properties of these glasses should be studied in order to understand the physicochemical properties of these systems [7].

In doped vitreous silicas, the major portion of nitrogen atoms enters into the glass structure as $N(–Si\equiv)_3$ or $H–N(–Si\equiv)_2$ units, in which the N–Si≡ and N–H groups replace lattice oxygen atoms (the N–H group and the O atom are isoelectronic systems). The formation of ordinary chemical bonds between nitrogen and oxygen atoms in vitreous silicas is improbable because of the comparatively low strength of the N–O bond in the $\equiv Si_2N–O–Si\equiv$ unit.

In this paper, the results of experimental and quantum-chemical studies of the structure and reactivity of nitrogen-containing paramagnetic centers in vitreous silica (on the surface and in the bulk) are presented. Data on the structure of a defect containing a dopant atom can be obtained by EPR spectroscopy in the case that this atom either occurs in a state with an unusual coordination (two-coordinated nitrogen atom) or else occurs in the nearest environment of another paramagnetic center. Paramagnetic centers with an unpaired electron localized on the three-coordinated silicon atom are formed in vitreous silica under exposure to various factors [8–10]. In the presence of nitrogen atoms in glass, a portion of these atoms can occur as the $(\equiv Si–O–)_2Si^{\bullet}(–N<)$ structure. However, to the best of the author's knowledge, the occurrence of these centers in nitrogen-doped vitreous silica has never been discussed in the literature. Thus, the occurrence of centers similar to $(>N–)_3Si^{\bullet}$ [11, 12] and paramagnetic centers in which the nitrogen atom is coordinated to four silicon atoms [13, 14] in these glasses was assumed; however, the above defect was not mentioned. In this paper, data on two paramagnetic defects of this kind, $(\equiv Si–O–)_2Si^{\bullet}(–NH_2)$ and $(\equiv Si–O–)_2Si^{\bullet}(–N(Si\equiv)_2)$, are reported.

The $\equiv Si–N^{\bullet}–Si\equiv$ and $\equiv Si–N^{\bullet}–H$ radicals containing a two-coordinated nitrogen atom belong to another type of paramagnetic center studied in this work. The $\equiv Si–N^{\bullet}–Si\equiv$ centers were identified by EPR spectroscopy in sodium silicate glass [15]. More recently, a similarly shaped EPR signal was also observed in nitrogen-doped vitreous silicas by other research groups [14, 16]. Centers similar to $\equiv Si–N^{\bullet}–Si\equiv$ were also obtained on the surface of vitreous silica. This allowed us to study their reactivity toward CO and H_2 molecules. The first data on the physicochemical characteristics of $\equiv Si–N^{\bullet}–H$ radicals were published elsewhere [17].

The results of quantum-chemical calculations of model low-molecular systems were used for the interpretation of the experimental data, including radiospectroscopic data. These calculations performed on an appropriate theoretical level give quantitative data on the spectroscopic, in particular, radiospectroscopic, characteristics of test systems and on the thermochemistry of processes with their participation [18, 19].

0023-1584/05/4604-0578 © 2005 MAIK "Nauka/Interperiodica"

EXPERIMENTAL

In this study, various techniques were used for introducing nitrogen into the composition of vitreous silica. In one of these, nitrogen-doped vitreous silicas $SiO_2(N)$ were prepared using a plasma-chemical SPCVD technology [20, 21]. According to the results of elemental analysis, these samples contained 3–5% nitrogen and ~1% chlorine.

Paramagnetic centers in the samples of nitrogen-doped vitreous silica were obtained by UV (193 nm) irradiation, γ-irradiation, or by the mechanical destruction of the samples in an inert atmosphere. The $SiO_2(N)$ samples were γ-irradiated at room temperature; the radiation dose was ~10 MGy. The sample was a cylinder ~3 mm in diameter and ~10 mm in height.

The UV irradiation was performed using an ArF laser with a radiation wavelength of 193 nm at room temperature. The sample as a rectangular prism 4 mm in height and 2×2 mm in cross section was irradiated on one or two opposite sides to a dose of no higher than 50 kJ/cm^2 at a dose rate of 10 W/cm^2.

The mechanical destruction of the $SiO_2(N)$ samples was performed in special vessels of vitreous silica (chamber volume of ~20 cm^3) filled with silica balls (15 balls ~3 mm in diameter). The sample was coarsely preground, and the fraction with a particle size of no greater than 1 mm was taken. This powder (~0.5 g) was placed in a quartz vessel, which was attached to a vacuum system. The sample was treated at 950 K by triply heating in oxygen (10^3 Pa) and evacuating at the specified temperature for burning organic surface impurities. Next, the sample was cooled to room temperature; the ampule was filled with an inert gas (10^3 Pa of helium), sealed off from the high-vacuum system, and fixed in an electromechanical vibrator. Disintegration was performed at room temperature. The vibrator frequency was 50 Hz, and the power density of the grinding apparatus was about 10^3 W/kg. As a result of the mechanical treatment (60 min), the specific surface area of the powder increased to 10 m^2/g (BET measurements using the low-temperature (77 K) adsorption of argon). After the mechanical treatment, the ampule with the sample was annealed in an atmosphere of helium at 700 K (15 min). This improved the resolution of the detected EPR signals without a considerable decrease in the concentration of paramagnetic centers. The effect observed was related to structural relaxation in the mechanically activated material, which was accompanied by a decrease in the contribution of nonuniform broadening to the width of EPR signals [22]. Next, the powder was transferred to a quartz cell for measuring EPR spectra, which was attached to a vacuum system (all of these operations were performed in the absence of contact of the sample with atmospheric air). The procedure in use provided an opportunity to measure the EPR spectra of a sample in a vacuum or controlled gas atmosphere (CO, O_2, H_2, etc.) with the simultaneous measurement of the amount of adsorbed molecules [9].

The other technique for the production of nitrogen-containing paramagnetic centers was based on the chemical modification of defects stabilized on the surface of highly dispersed activated silica (Aerosil) [23]. The experiments were performed with the powders of highly dispersed Aerosil A-300 (the initial specific surface area was ~300 m^2/g). The procedure for the thermochemical activation of a silica surface, which resulted in a dramatic increase in its chemical activity (the formation of so-called reactive silica (RSi)), was developed by Morterra and Low [24, 25]. To obtain nitrogen-containing paramagnetic centers, NH_3 (ND_3) was used as a modifier molecule. All of the experiments were performed under conditions of a high vacuum or controlled atmosphere.

The pressure of gases and vapors in the system was monitored using a Pirani gage.

The EPR spectra of the samples were measured on an EPR-20 X-band instrument (Semenov Institute of Chemical Physics, Russian Academy of Sciences) at 300 or 77 K.

The quantum-chemical calculations were performed using the Gaussian-94 program [26]. Fluorine-substituted molecular models of the defects of vitreous silica, in which ≡Si–O– groups were replaced by F atoms, were used in the calculations. For example, the $F_2Si^{\bullet}(-NH_2)$ radical served as a model of the $(\equiv Si–O–)_2Si^{\bullet}(-NH_2)$ radical. As found previously [19, 27], various types of paramagnetic or diamagnetic intrinsic and impurity defects in silica and their fluorine-substituted low-molecular analogs exhibited similar physicochemical characteristics. The reasons for this similarity are due to the spatial localization of the electronic states of the defect atom and to the fact that the F atom and the ≡Si–O– group have similar substituent effects on the properties of a silicon atom bound to them. The molecular structures were optimized using the gradient approximation of the density functional theory (DFT) at the UB3LYP/6-311G(d,p) or UB3LYP/6-311G(2d,2p) level [28, 29]. Vibrational spectra were calculated for all of the optimized structures. Transition states were characterized by a negative eigenvalue of the Hessian matrix. The heats of reactions at 0 K $\Delta H(0\text{ K}) = \Delta E(0\text{ K}) + \Delta(ZPE)$ (here, $\Delta E(0\text{ K})$ and $\Delta(ZPE)$ are differences between the energies and zero-point energies of the initial reactants and products, respectively) were calculated both at the DFT level and at the G2MP2//B3LYP/6-311G(d,p) level [30]. The latter was developed for calculating the heats of the formation of compounds, and it reproduced the thermochemical characteristics of processes better than DFT

Table 1. Radiospectroscopic characteristics of $(\equiv Si–O)_2Si^{\bullet}(NH_2)$ (experimental) and $F_2Si^{\bullet}(NH_2)$ (calculated) radicals

HFC tensor	a_{iso}, G		b_1, G		b_2, G		b_3, G	
	experimental	calculated	experimental	calculated	experimental	calculated	experimental	calculated
^{29}Si	–377 ± 1	–391.4	–37.2 ± 1	–40.6	18.6 ± 0.5	20.7	18.6 ± 0.5	19.9
^{14}N	12.8 ± 0.3	8.8	2.6 ± 0.3	6.2	–1.9 ± 0.3	–3.2	–0.7 ± 0.3	–3.0
^{1}H	$\lvert a_{iso}\rvert \le 2$	–3.8	–	5.3	–	–4.2	–	–1.3

did. The enthalpies of compounds at 0 K were calculated from the equation

$$E(\text{G2MP2(0K)}) = E(\text{QCISD(T, E4T)/6–311G(d,p)}) + (E(\text{MP2/6–311 + G(3df,2p)}) - E(\text{MP2/6–311G(d,p) + ZPE} - 0.005n(\beta) - 0.0009(n(\alpha) - n(\beta)).$$

The first term in this expression is the energy of the structure at the QCISD(T,E4T)/6-311G(d,p) level [26]; the second term is a change in the energy of the system when the size of the basis set (the second parentheses) is increased; the third term is the zero-point energy calculated at the DFT(B3LYP/6-311G(d,p)) level; and the other terms are a semiempirical so-called higher level correction [30], in which $n(\beta)$ is the number of β electrons in the system and $(n(\alpha) - n(\beta))$ is the difference between the numbers of α and β electrons.

RESULTS AND DISCUSSION

1.1. $(\equiv Si–O)_2Si^{\bullet}(NH_2)$ radicals. These radicals were obtained as a product of the following two-step process that occurred on the activated surface of silica containing defects of two types (paramagnetic $(\equiv Si–O)_3Si–O^{\bullet}$ and diamagnetic $(\equiv Si–O)_2Si$ (for details, see [18])):

$$(\equiv Si–O)_3Si–O^{\bullet} + NH_3 \longrightarrow (\equiv Si–O)_3Si–O–H + {}^{\bullet}NH_2, \quad (I)$$

$$(\equiv Si–O)_2Si: + {}^{\bullet}NH_2 \longrightarrow (\equiv Si–O)_2Si^{\bullet}(NH_2) \quad (II)$$

Oxy radicals played the role of a generator of $^{\bullet}NH_2$ radicals (reaction (I)). The latter added to diamagnetic surface centers containing a two-coordinated silicon atom (reaction (II)). The structure of the resulting radical was identified by EPR spectroscopy (Table 1 summarizes the radiospectroscopic characteristics).

A change in the detection temperature (from 300 to 77 K) caused irreversible changes in the shapes of EPR spectra. This suggests the unfreezing of internal motions in the radical, which affect its radiospectroscopic characteristics.

Figure 1a shows the optimized structure of the $F_2Si^{\bullet}(NH_2)$ radical, which served as a molecular model of the $(\equiv Si–O)_2Si^{\bullet}(NH_2)$ surface center. According to calculation data, this is the only structure corresponding to a local minimum in the potential energy surface of the system. The environment of the nitrogen atom in the radical is pyramidal with the HNSiH torsion angle equal to 145.2° (if the $Si–NH_2$ group is made planar, the energy of the system increases by 0.6 kcal/mol). In the NH_3 molecule, this angle is noticeably smaller (~110°), and the energy consumption required for converting the molecule into a planar form is ~6 kcal/mol [31]. Thus, the replacement of an H atom by an Si atom resulted in the flattening of the $Si–NH_2$ fragment.

The radical geometry was characterized by the position of one of the protons of the NH_2 group, the torsion angle φ, which indicates the deviation of the H1 atom from the plane formed by the N atom and the bisecting line of the FSiF angle (the Si–X line in Fig. 1a; clockwise angle; 0^0 corresponds to the *cis* arrangement of H1, N, Si, and X). For the equilibrium conformation of the radical (C_s symmetry), φ = 83.6°.

The barrier height for the intramolecular rotation of the NH_2 group in the $F_2Si^{\bullet}(NH_2)$ radical is no higher than 2 kcal/mol (Fig. 1b). Energy maximums correspond to radical geometries in which one of the H atoms lies in the plane formed by the N atom and the bisecting line of the FSiF angle (φ = 0° and 180°). When the H1 atom intersects this plane (at the top or bottom), the inversion of the $SiNH_2$ group in which the H2 atom is shifted to a considerable distance becomes energetically favorable. The second region of the inversion of the SiNH1H2 group occurs in another range of torsion angles: near the positions that correspond to an eclipsed arrangement of Si–F1 and N–H1 bonds. In this region, on the contrary, considerable shifts of the H1 atom are accompanied by much smaller shifts of the H2 atom. Thus, as the NH_2 group rotates, the N atom successively occurs at different sides of the plane formed by the Si, H, and H atoms. This resembles a butterfly flapping its wings (H atoms): as a result of a full turn, the NH_2 group twice "flapped its wings" (H atoms). Thus, the rotation of the NH_2 group in the radical cannot be considered as the motion of a rigid rotator: the displacements of H atoms are accompanied by considerable changes in other geometry characteristics, primarily, the HNSiH torsion angle.

Table 1 summarizes the tensors of the hyperfine interaction of an unpaired electron with magnetic nuclei calculated for the equilibrium radical structure. Figure 1c shows the dependence of isotropic hyperfine coupling (HFC) constants for an unpaired electron with ^{14}N and ^{1}H nuclei in the radical on the rotation angle of the NH_2 group. In this case, the value of $a_{iso}(^{29}Si)$ changed from –39.1 to –41.5 G.

A minimum value of the constant $a_{iso}(^{14}N)$ corresponds to the radical geometry that is insignificantly different from its equilibrium conformation. Therefore, the value of this constant will increase with detection temperature. The temperature dependence of the isotropic HFC constant can be written in the form

$$a_{iso}(T) = \int \exp[-E(\varphi, T)/RT] \times a_{iso}(\varphi)d\varphi / \int \exp[-E(\varphi, T)/RT]d\varphi.$$

With the use of the $E(\varphi)$ and $a_{iso}(\varphi)$ functions shown in Fig. 1, the constant $a_{iso}(^{14}N)$ was calculated to be 11.2 G at 300 K. In the high-temperature limit (free rotation of the NH_2 group), $a_{iso}(^{14}N) = 13.6$ G. Note that an increase in the displacement amplitude of the NH_2 group with temperature will partially average the anisotropic component of the HFC tensor of an unpaired electron with the nitrogen nucleus to improve the agreement between calculated and experimentally found values.

Let us consider the HFC constants for an unpaired electron and the protons of the NH_2 group. For the equilibrium structure of the radical, the calculated values are $a_{iso}(H1) = a_{iso}(H2) = –3.8$ G. Figure 1c illustrates the calculation results for the dependence of the constant $a_{iso}(^{1}H)$ on the rotation angle of the NH_2 group. As the temperature was raised and the displacement amplitude of the NH_2 group increased, the absolute value of this constant decreased, passed through zero, and then became positive. In the high-temperature limit (free rotation of the NH_2 group), $a_{iso}(^{1}H) = 2.75$ G; however, it was far from this region at 300 K. With the use of the $E(\varphi)$ and $a_{iso}(\varphi)$ functions shown in Fig. 1, the calculated value of the constant was –0.9 G at 300 K. As noted previously [18], the hyperfine interaction of an unpaired electron with protons does not manifest itself as a resolved hyperfine structure (at 300 K) in the EPR spectrum of the $(\equiv Si–O)_2Si^{\bullet}(NH_2)$ radical.

Thus, the results of the quantum chemical calculations of the radiospectroscopic characteristics of the $F_2Si^{\bullet}(NH_2)$ radical as a model system are consistent with the experimental data.

1.2. $(\equiv Si–O)_2Si^{\bullet}–N(Si\equiv)_2$ radical. Figure 2 demonstrates the EPR spectra of the samples of nitrogen-doped vitreous silica after mechanical destruction and UV irradiation (*RT*, λ = 193 nm). An increase in the UV-radiation dose (to 50 kJ/cm^2) was accompanied by an increase in the concentration of the resulting paramagnetic centers without considerable changes in the shape of the signal. The EPR signal of the paramagnetic centers formed upon the γ-irradiation of the samples was similar to that shown in Fig. 2b for UV-irradiated glass.

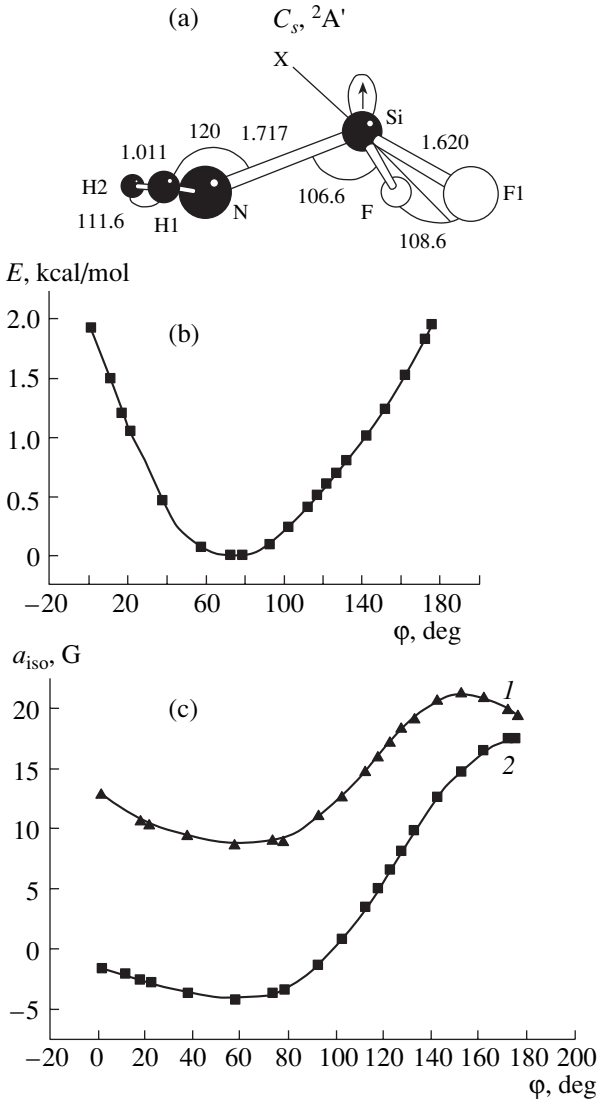

Fig. 1. $F_2Si^{\bullet}–NH_2$ radical: (a) optimized structure; (b) dependence of the energy of the radical on the rotation angle φ = H1NSiX of the NH_2 group (the pseudoatom X lies in the bisecting line of the F–Si–F angle); and (c) dependence of the isotropic constants of the HFC of an unpaired electron with (*1*) ^{14}N and (*2*) ^{1}H nuclei in the radical on the rotation angle φ of the NH_2 group.

Based on the available published data, the central single anisotropic line in the EPR spectra shown in Fig. 2 should be assigned to radicals in which the unpaired electron is localized on the three-coordinated silicon atom. Weeks [8] supposed its structure to be $(\equiv Si–O)_3Si^{\bullet}$. In the case of surface centers, the presence of three silicon atoms in the coordination sphere of the central (three-coordinated) silicon atom was dem-

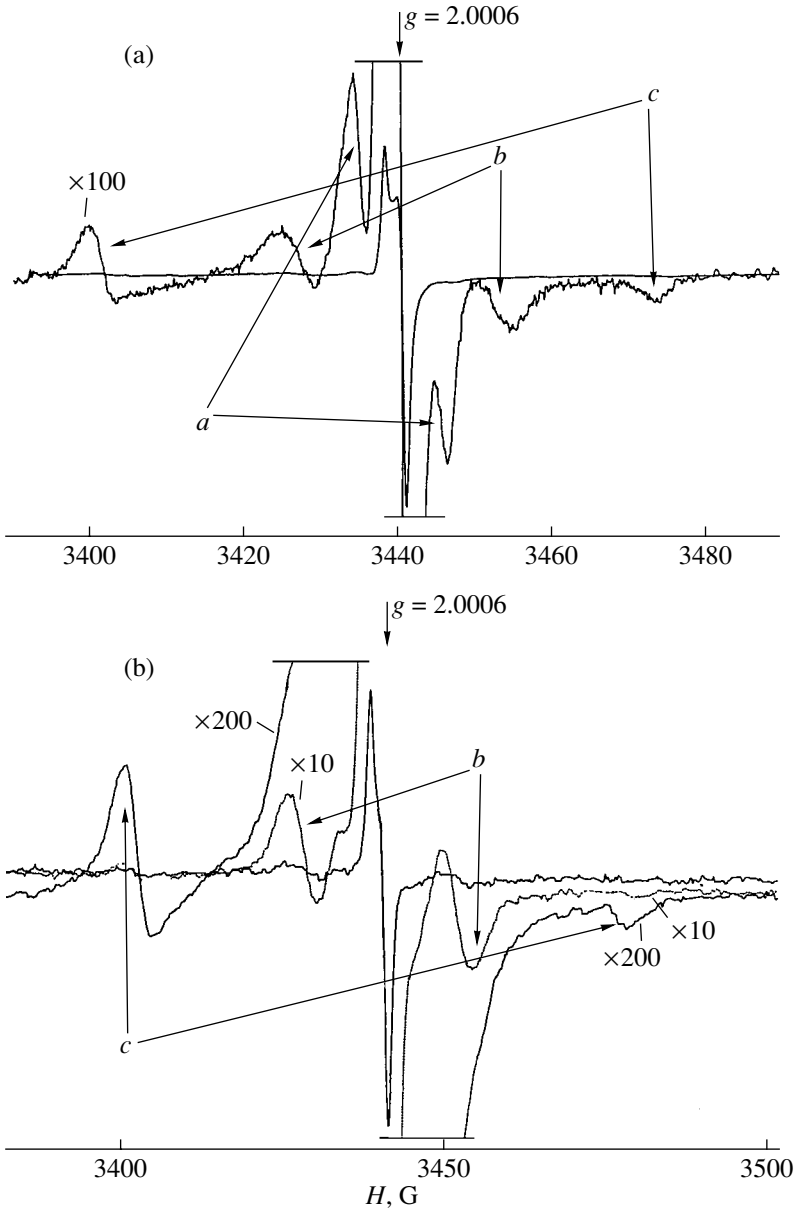

Fig. 2. EPR spectra of paramagnetic centers in nitrogen-doped SiO_2 samples: (a) after mechanical treatment at 300 K; arrows indicate lines due to (*a*) $(\equiv{}^{29}Si–O)_3{}^{28}Si^{\bullet}$, (*b*) $(\equiv{}^{28}Si–O)_2{}^{28}Si^{\bullet}–{}^{14}N<$, and (*c*) $\equiv{}^{28}Si–{}^{14}N^{\bullet}–{}^{28}Si\equiv$ radicals; (b) after UV irradiation (λ = 193 nm; 300 K); arrows indicate lines due to (*b*) $(\equiv{}^{28}Si–O)_2{}^{28}Si^{\bullet}–{}^{14}N<$ and (*c*) $^{28}Si–{}^{14}N^{\bullet}–{}^{28}Si\equiv$ radicals. The spectra were measured at 300 K.

onstrated experimentally [32]. Two lines separated by ~10.5 G, which are marked *a* in Fig. 2a, are due to the interaction of the unpaired electron with ^{29}Si nuclei (I = 1/2; natural abundance of 4.7%) in the coordination sphere of a defect. Relevant data for bulk centers are unavailable.

In all cases, along with the main central signal, the EPR spectra also exhibited two extra lines separated by of ~25 G (marked *b* in Fig. 2). The ratio between the amplitudes of central (due to $(\equiv Si–O)_3Si^{\bullet}$ radicals) and side components depended only slightly on the preparation method (irradiation or mechanical treatment).

After heating a mechanically activated sample, which improved the resolution of the EPR spectrum, it was evident that the side components are slightly asymmetric due to g-tensor anisotropy with the value of $g_{\perp}$ = 2.0007 (measured between the intersection points of components with the zero line). The value of $g_{\parallel}$ is difficult to determine because of the low signal resolution. However, based on the shape of the spectrum, it can be

concluded that $g_\perp < g_\parallel$ and is close to the value typical of $(\equiv Si–O)_3Si^\bullet$ radicals (2.0018). Thus, the g tensor of the signal is characteristic of paramagnetic centers in which the unpaired electron is localized on the three-coordinated silicon atom [18, 27]. On the other hand, the isotropic HFC constant for the unpaired electron with the nitrogen nucleus in the $(\equiv Si–O)_2Si^\bullet(NH_2)$ radical is ~13 G; that is, the distance between the edge lines of the triplet spectrum of this radical is close to 25 G, and it exhibits the main g-tensor values close to the above values. The above experimental data suggest that the observed lines are part of a triplet EPR signal with splitting between components of ~12.5 G. This signal is due to the interaction of the unpaired electron with the nitrogen nucleus and belongs to the $(\equiv Si–O)_2Si^\bullet(N(Si\equiv))_2$ radical. The central component of this signal is masked by the more intense spectrum of $(\equiv Si–O)_3Si^\bullet$ radicals.

Figure 3 demonstrates the optimized structure of the low-molecular $F_2Si^\bullet–N(SiF_3)_2$ radical, which served as a molecular model of the $(\equiv Si–O)_3Si^\bullet–N(Si\equiv)_2$ radical in vitreous silica. According to the results of calculations, the $SiNSi_2$ fragment in the radical is planar, unlike the $SiNH_2$ group in the $F_2Si^\bullet–NH_2$ radical. Thus, the pyramidality of the N atom decreases in the order NH_3, $\equiv Si–NH_2$, $\equiv Si–NH–Si\equiv$, and $NSi\equiv_3$, and the last two members of this series are planar. Figure 3 shows the potential energy profile for the rotation of the $N(SiF_3)_2$ group about the $F_2Si–N$ bond. Figure 3 also demonstrates the isotropic HFC constants for an unpaired electron and ^{29}Si and ^{14}N nuclei. Unlike the $F_2Si^\bullet–NH_2$ radical, this rotation is not accompanied by a noticeable change in the HFC constant with the nitrogen nucleus. This is typical of the nitrogen atom in a planar coordination. According to calculations, in the case of the $F_2Si^\bullet–NH_2$ radical in which the $Si–NH_2$ fragment was artificially made planar, the isotropic HFC constant of an unpaired electron with the nitrogen nucleus was practically independent of the rotation angle of the NH_2 group. Note that the calculated HFC constant with the nitrogen nucleus is consistent with the experimentally measured constant in the $(\equiv Si–O)_2Si^\bullet–N(Si\equiv)_2$ radical.

The anisotropy of the HFC tensor of the unpaired electron with the nitrogen nucleus in the $(\equiv Si–O)_2Si^\bullet–N(Si\equiv)_2$ radical results in different broadenings of central ($M(N) = 0$) and edge ($M(N) = \pm 1$) components of the triplet spectrum. As a result, the central component of the triplet is better resolved, as can be seen in the EPR spectrum of the $(\equiv Si–O)_2Si^\bullet(NH_2)$ radical, by way of example [18]. The anisotropic component of the HFC tensor of the unpaired electron with the nitrogen nucleus in the $(\equiv Si–O)_2Si^\bullet–N(Si\equiv)_2$ radical was estimated from the width of the edge components of the

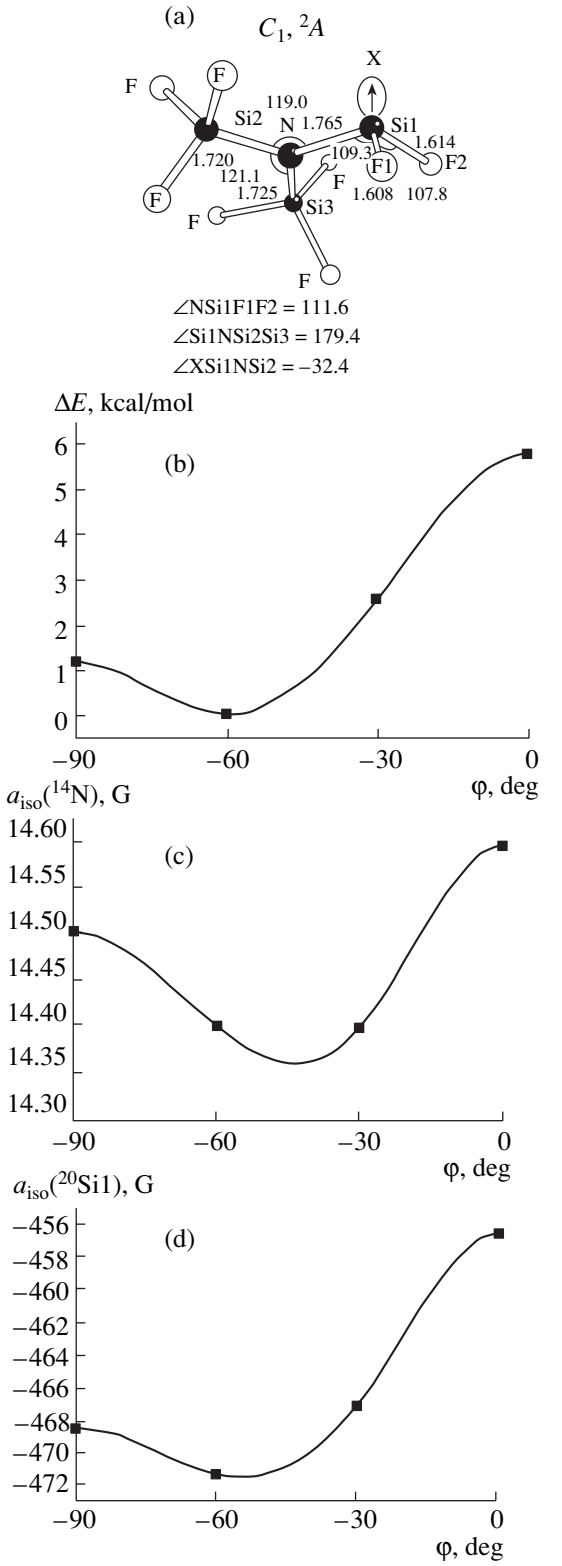

Fig. 3. $F_2Si^\bullet_\alpha–N(Si_\beta F_3)_2$ radical: (a) optimized structure; (b) dependence of the energy of the radical on the rotation angle φ = XSi1NSi2 of the $N(SiF_3)_2$ group (the pseudoatom X lies in the axis of the orbit of the unpaired electron); and dependence of the isotropic constants of the HFC of an unpaired electron with (c) ^{14}N and (d) $^{29}Si_\alpha$ nuclei in the radical on the rotation angle of the $N(SiF_3)_2$ group.

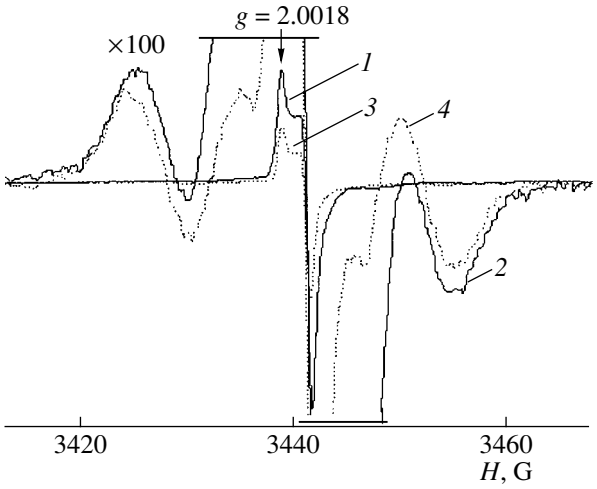

Fig. 4. EPR spectra of (*1*, *2*) a mechanically activated sample of SiO_2(N) and (*3*, *4*) this sample after contact with oxygen at 300 K (measurements at 300 K; spectra *2* and *4* were recorded at a higher amplification).

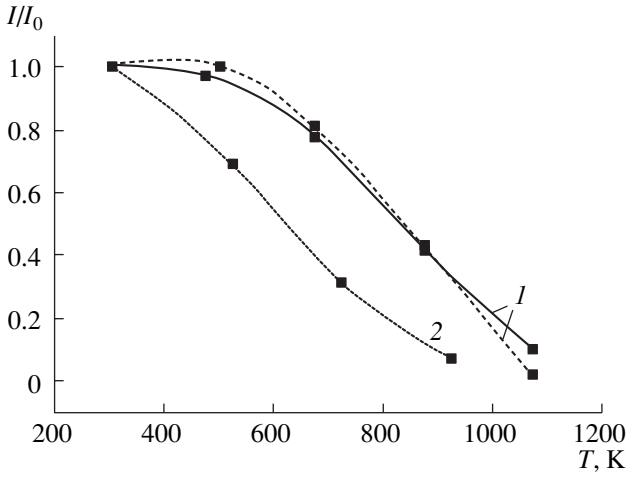

Fig. 5. Curves of the thermal annealing of paramagnetic centers in (*1*) UV- and (*2*) γ-irradiated SiO_2(N) samples (the exposure time at each temperature was 10 min). I/I_0 is the relative intensity of the EPR signals of paramagnetic centers, where $I_0 = I$ (300 K).

triplet spectrum (Fig. 2a): it was no higher than a few gausses. The $(\equiv Si–O)_2Si^{\bullet}–N(Si\equiv)_2$ is rigidly fixed in the structure of vitreous silica, and its intramolecular mobility, which can average this anisotropy, is restricted. The result obtained is consistent with quantum chemical calculation data. According to these data, for the equilibrium configuration of the $F_2Si^{\bullet}–N(SiF_3)_2$ radical, the main tensor values for the anisotropic HFC with the nitrogen nucleus are –1, –1.5, and 2.5 G.

The constants of HFC with $^{29}Si_\beta$ atoms are sensitive to the spatial arrangement of the $N(SiF_3)_2$ fragment in the $F_2Si^{\bullet}_\alpha–N(Si_\beta F_3)_2$ (the angle of rotation about the Si_α–N bond). According to calculation data, the isotropic HFC constants vary from 0 to –13 G. A maximum absolute value of the constant corresponds to the *trans* configuration of a fragment of $^{29}Si_\beta$, N, Si_α, and X (see Fig. 3a). The constant of HFC of an unpaired electron with the $^{29}Si_\beta$ atom in the $>Si^{\bullet}_\alpha–O–Si_\beta\equiv$ radical exhibited a similar structural sensitivity [27, 32].

Based on the assumption that the EPR signal shown in Fig. 2 is a superposition of singlet and triplet spectra, the fraction of a triplet signal in the total spectrum was estimated at (15 ± 5)%. According to elemental analysis data, the nitrogen content of glass was (4–5)%. Under the assumption that nitrogen substitutes for an oxygen atom in the coordination sphere of the $(\equiv Si–O)_3Si^{\bullet}$ radical in a random fashion, the fraction of nitrogen-containing centers is 3 × (0.04–0.05) = 0.12–0.15, which is consistent with the above result.

Figure 4 shows changes in the shape of EPR signals due to paramagnetic centers in a mechanically activated sample of nitrogen-doped vitreous silica after coming into contact with oxygen molecules. The concentration of $(\equiv Si–O)_3Si^{\bullet}$ radicals decreased (Fig. 4, spectra *1*, *2*) because a portion of these radicals stabilized on the solid surface reacted with oxygen molecules. Peroxide radicals ($\equiv Si–O–O^{\bullet}$) are the products of this reaction [27, 32]. These radicals exhibit a much broader EPR spectrum; therefore, their appearance cannot be detected in the EPR spectrum shown. It is interesting to note that, unlike $(\equiv Si–O)_3Si^{\bullet}$ radicals whose concentration decreased more than two times, no changes were detected in the amplitude of lines due to $(\equiv Si–O)_2Si^{\bullet}–N(Si\equiv)_2$ radicals (Fig. 4, spectra *2*, *4*). By this is meant that the major portion of paramagnetic centers of this type formed upon the mechanical treatment of glass is stabilized in a near-surface layer of the material rather than on the surface. The question as to the reasons for the effect observed remains open.

Figure 5 illustrates the thermal decay of paramagnetic centers on the heating of UV- and γ-irradiated samples. The process was not accompanied by considerable changes in the shape of EPR signals; that is, differences in the structures of the coordination spheres of $(\equiv Si–O)_3Si^{\bullet}$ and $(\equiv Si–O)_2Si^{\bullet}–N(Si\equiv)_2$ paramagnetic centers have no effect on the thermal stability. However, note that the thermal stability of paramagnetic centers in the UV-irradiated sample was much higher.

2.1. $\equiv Si–N^{\bullet}–Si\equiv$ radical. Based on the characteristic shape of edge components in the EPR spectra of products formed by the mechanical treatment, UV irradiation (see Fig. 2), or γ-irradiation of nitrogen-doped vitreous silica, these components were assigned to $\equiv Si–N^{\bullet}–Si\equiv$ radicals (in the test samples, the central part of the EPR spectrum of these radicals was masked by the intense signal of silicon-centered radicals). Mackey *et al.* [15] recorded an individual EPR spectrum of $\equiv Si–N^{\bullet}–Si\equiv$ radicals in sodium silicate glass.

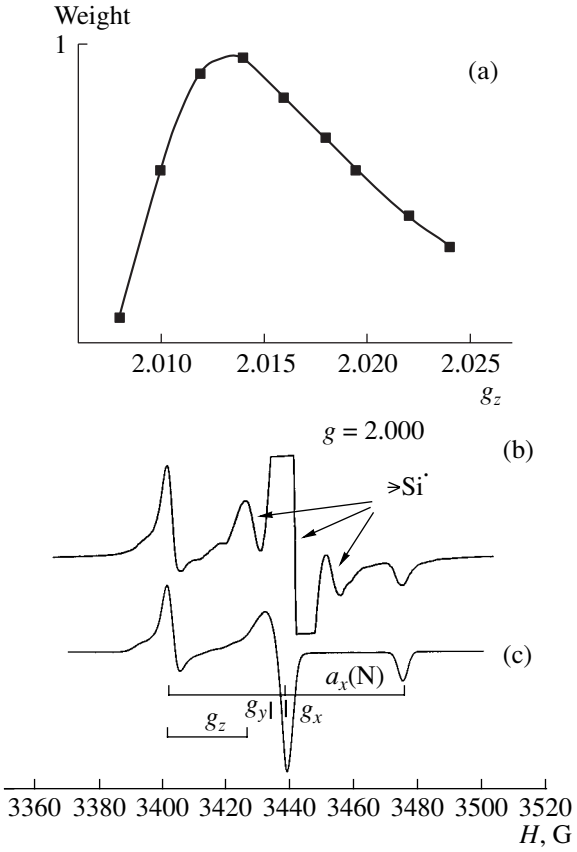

Fig. 6. ≡Si–˙N –Si≡ radicals in vitreous silica: (a) distribution function (weight) of the number of ≡Si–˙N –Si≡ radicals in sodium silicate glass characterized by a certain value of the g-tensor component g_z [15]; (b) (*1*) the EPR spectrum of radicals in the products of mechanical degradation of SiO_2(N) silica and (*2*) the simulated EPR spectrum of ≡Si–˙N –Si≡ radicals (the spin-Hamiltonian parameters are specified in Table 2).

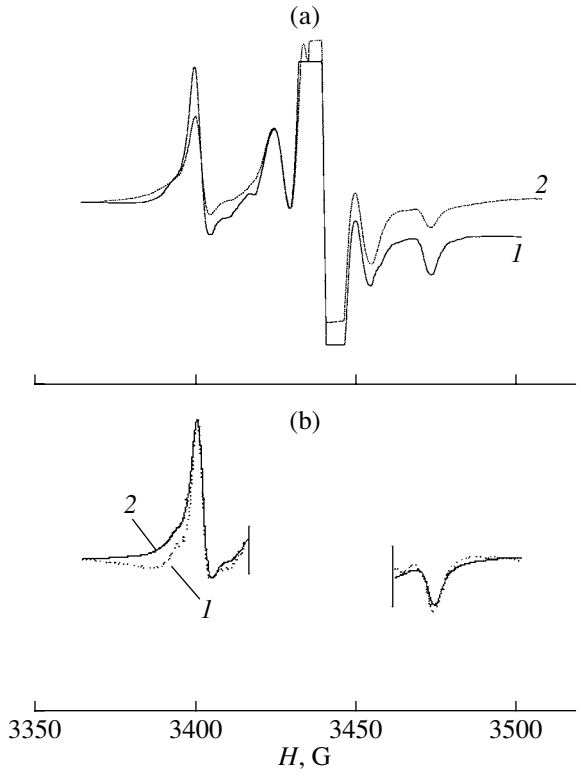

Fig. 7. EPR spectra of surface and bulk ≡Si–˙N –Si≡ radicals in mechanically activated vitreous silica: (a) (*1*) activated sample and (*2*) this sample treated with oxygen at 300 K; (b) comparison between the shapes of edge components in the EPR spectra of (*1*) surface and (*2*) bulk ≡Si–˙N –Si≡ radicals.

Other evidence of the specified structure of the resulting radicals based on a study of their chemical properties is given below in Sections 4 and 5.

The positions of the specified lines are practically independent of the temperature at which the EPR spectrum was measured (77 or 300 K), and the intensity of these lines obeys the Curie law. The relative fraction of centers of this type in the total spectrum increased on measuring the EPR signal at enhanced microwave power levels. Consequently, saturation effects for these paramagnetic centers appeared at noticeably higher microwave power levels than those for radicals containing a three-coordinated silicon atom, $(\equiv Si–O)_3Si^{\bullet}$ and $(\equiv Si–O)_2Si^{\bullet}–N(Si\equiv)_2$. The fractions of $\equiv Si–N^{\bullet}–Si\equiv$ radicals in the total paramagnetic centers detected by EPR spectroscopy were dramatically different depending on the preparation method. A maximum value of 0.40 ± 0.15 of the total amount of paramagnetic centers was observed in mechanically activated silica samples (the major portion of the other centers consisted of $(\equiv Si–O)_3Si^{\bullet}$ radicals). This value in UV- and γ-irradiated samples was lower by almost one order of magnitude. The fraction of $\equiv Si–N^{\bullet}–Si\equiv$ radicals in the total spectrum was calculated from the intensity of a well-resolved high-field component in the experimentally observed EPR signal. The ratio of the intensity of this component to the total intensity of the theoretically calculated EPR spectrum of the $\equiv Si–N^{\bullet}–Si\equiv$ radical served as a reference (Fig. 6b).

The contact of mechanically activated vitreous silica samples containing $\equiv Si–N^{\bullet}–Si\equiv$ radicals with molecular oxygen from a gas phase (Fig. 7a) was accompanied by a decrease in the intensity of the EPR signal (by 25 to 50% depending on the duration of mechanical treatment). This fact indicates that a portion of radicals was accessible to gas-phase molecules; that is, these radicals were stabilized on the sample surface. In this manner, the EPR spectra of surface and bulk centers can be separated (the latter are stabilized in near-surface layers of the material [9], and they are inaccessible to molecules from a gas phase). Figure 7b shows a fragment (lines on the right) of the EPR spectrum of

Table 2. Radiospectroscopic characteristics of the nitrogen-containing paramagnetic centers studied in this work

Radical structure	Main g- and a-tensor values, G			
$>{}^{29}Si^{\bullet}({}^{14}NH_2)$	$g_x = 2.0018 \pm 0.0002$	$a_x({}^{14}N) = 15.4 \pm 0.2$	$a_{\parallel}({}^{29}Si) = -414 \pm 2$	
300 K	$g_y = 2.0011 \pm 0.0002$	$a_y({}^{14}N) = 10.9 \pm 0.2$	$a_{\perp}({}^{29}Si) = -358.4 \pm 2$	
	$g_z = 2.0002 \pm 0.0002$	$a_z({}^{14}N) = 12.1 \pm 0.2$	$a_{\perp}({}^{29}Si) = -358.4 \pm 2$	
	$g_{iso} = 2.0010 \pm 0.0002$	$a_{iso}({}^{14}N) = 12.8 \pm 0.2$	$a_{iso}({}^{29}Si) = -377 \pm 2$	
$\equiv{}^{29}Si-{}^{14}N^{\bullet}-{}^{1}H$	$g_{\parallel} \cong 2.012$	$a_{\parallel}({}^{14}N) = 0 \pm 1$	$a_{\parallel}({}^{1}H) \cong -17 \pm 1$	
77 K	$g_{\perp} \cong 2.0043$	$a_{\perp}({}^{14}N) = 18 \pm 1$	$a_{\perp}({}^{1}H) \cong -21.5 \pm 1$	
	$g_{iso} = 2.0069$	$a_{iso}({}^{14}N) = 12 \pm 1$	$a_{iso}({}^{1}H) \cong -20 \pm 1$	$a_{iso}({}^{29}Si) = 16 \pm 2$
$\equiv Si-{}^{14}N^{\bullet}-Si\equiv$*	$g_x = 2.0019$ (2.0039)		$a_x({}^{14}N) = 36$ (36)	
77 K	$g_y = 2.0039$ (2.0026)		$a_y({}^{14}N) \cong 2$ (2)	
	$g_z = 2.0078$–2.0238 (2.006–2.02)		$a_z({}^{14}N) \cong 2$ (2)	
$(\equiv Si-)_2{}^{14}N-{}^{13}C^{\bullet}=O$	$g_{\parallel} = 1.9984$	$a_{\parallel}({}^{14}N) = 25.7$	$a_{\parallel}({}^{13}C) = 206.8$	
300 K	$g_{\perp} = 2.0036$	$a_{\perp}({}^{14}N) = 24.25$	$a_{\perp}({}^{13}C) = 166$	
	$g_{iso} = 2.0019$	$a_{iso}({}^{14}N) = 24.7$	$a_{iso}({}^{13}C) = 179.6$	
$\equiv{}^{29}Si-{}^{14}NH-{}^{13}C^{\bullet}=O$	$g_x = 1.9983 \pm 0.0002$	$a_x({}^{14}N) = 29.0 \pm 0.5$	$a_x({}^{1}H) = 32.0 \pm 0.2$	$a_{\parallel}({}^{13}C) = 188 \pm 2$
trans configuration	$g_y = 2.0028 \pm 0.0002$	$a_y({}^{14}N) = 30.4 \pm 0.5$	$a_y({}^{1}H) = 30.4 \pm 0.5$	$a_{\perp}({}^{13}C) = 158 \pm 1$
of O, C, N, and Si atoms	$g_z = 2.0043 \pm 0.0002$	$a_z({}^{14}N) = 27.8 \pm 0.5$	$a_z({}^{1}H) = 27.8 \pm 0.5$	
77 K	$g_{iso} = 2.0018 \pm 0.0002$	$a_{iso}({}^{14}N) = 29.1 \pm 0.5$	$a_{iso}({}^{1}H) = 30.1 \pm 0.5$	$a_{iso}({}^{13}C) = 168 \pm 2$
$\equiv{}^{29}Si-{}^{14}NH-{}^{13}C^{\bullet}=O$				$a_{\parallel}({}^{13}C) = 201.5 \pm 1$
cis configuration				$a_{\perp}({}^{13}C) = 166 \pm 1$
of O, C, N, and Si atoms	$g_{iso} = 2.0020 \pm 0.0002$	$a_{iso}({}^{14}N) = 20.9 \pm 0.5$	$a_{iso}({}^{29}Si) = 32 \pm 1$	$a_{iso}({}^{13}C) = 178 \pm 2$
300 K				

* The spin distribution function with respect to g_z values was taken to consist of five fractions with $g_z = 2.0078$, 2.0118, 2.0158, and 2.0238, which have equal weights. Published data [15] are given in parentheses.

Table 3. Comparison between the experimental (e) and calculated (UB3LYP/6-311G**) (c) isotropic and anisotropic components of HFC constants (G) of nitrogen-centered radicals

Radical	$a_{iso}({}^{14}N)$	b_1	b_2	b_3	$a_{iso}({}^{1}H)$	b_1	b_2	b_3	$a_{iso}({}^{29}Si)$	b_1	b_2	b_3
$^{\bullet}NH_2$ (e) [37]	10.5	–	–	–	|24.0|	–	–	–				
(c)	7.4	31.4	–15.4	–16.0	–22.0	–3.8	7.2	–3.6				
$^{\bullet}NF_2$ (e) [38]	16.3 ± 1	32.6	–16.3	–16.3								
(c)	12.2	33.7	–16.4	–17.3								
$F_3Si-{}^{\bullet}NH$ (c)	7.2	29.0	–14.5	–14.5	–18.8	22	–18	–4	–17.3	1.0	0.4	–1.4
$F_2(HO)Si-{}^{\bullet}NH$ (c)	7.7	28.9	–14.5	–14.4	–20.4	21.9	–18.4	–3.4	–16.4	0.6	0.1	–0.7
$\equiv Si-{}^{\bullet}N-Si\equiv$ (e) [15]	13 ± 1	36	|2|	|2|							
$F_3Si-{}^{\bullet}N-SiF_3$ (c)	7.2	27.3	–13.5	–13.8					–14.5	0.7	0.2	–0.9

centers that disappeared upon contact between the sample and molecular O_2 at 300 K. It can be seen that the EPR spectra of surface and bulk radicals are similar (at least in this region).

Tables 2 and 3 summarize the radiospectroscopic characteristics of $\equiv Si-N^{\bullet}-Si\equiv$ radicals [15]. According to an analysis performed in this work (the measurement of EPR spectra at frequencies of 9.5, 16.3, and 34.9 MHz and a comparison of the signals with the results of a numerical simulation), particular groups of paramagnetic centers differed in the value of one of the g-tensor components: $2.008 \le g_z \le 2.024$ (Fig. 6a). This special feature was most clearly pronounced in the shape of a low-field component of the EPR spectrum of $\equiv Si-N^{\bullet}-Si\equiv$ radicals. Mackey *et al.* [15] related the observed differences in the values of the g_z component to differences in the Si–N–Si angles of radicals stabilized in a disordered solid (glass).

Published data [15] on the radiospectroscopic characteristics of $\equiv Si-N^{\bullet}-Si\equiv$ radicals in sodium silicate

glass formed a basis in the simulation of the detected EPR signal (Fig. 6c). Data consistent with the experimental results were obtained with the use of a spin Hamiltonian with parameters specified in Table 2. These parameters are somewhat different from published values [15]. Like Mackey *et al.* [15], the present author hypothesized that particular groups of paramagnetic centers differ in the value of the g_z component ($2.0078 \le g_z \le 2.0238$). Only in this case, the shape of the low-field component of the EPR spectrum, with an additional shoulder on its left-hand side, can be satisfactorily simulated (Fig. 6b).

2.2. Electronic structure of ≡Si–N˙–Si≡ radicals. The radiospectroscopic characteristics of a radical depend on its geometry and electronic structure. In the electronic ground state of ≡Si–N˙–Si≡ radicals (^2X), an unpaired electron is localized on the $2p_x$ AO of nitrogen, the axis of symmetry of which is perpendicular to the plain formed by the nitrogen atom and its two substituents (Fig. 8b). The lower electronically excited state is due to electron transfer from a lone pair of the nitrogen atom to a half-filled orbital occupied by an unpaired electron [15]. In this state (^2A), an unpaired electron is also mainly localized on the $2p_y$ AO of nitrogen, the axis of symmetry of which is oriented along the bisecting line of the Si–N–Si angle (Fig. 8b). In both of these states, the main portion of spin density is localized on the nitrogen atom. The occurrence of this excited state resulted in a shift of the g_z g-tensor component of the radical (the z axis (Fig. 8b) lies in the plane of the radical and is oriented approximately perpendicularly to the bisecting line of the Si–N–Si valence angle (the y axis)). This shift can be estimated from the following equation [33]:

$$\Delta g_z = g_z - g_e \cong 2\lambda c_1^2 c_2^2/\Delta E, \qquad (1)$$

where λ is the spin–orbital interaction constant for the N atom in the radical; c_1^2 and c_2^2 are the occupancies $2p_x$ and $2p_y$ AOs of nitrogen in the ground and lower electronically excited states, respectively; and ΔE is the energy difference between these states. Here, the two-level approximation is used and the effects of the next excited states of the radical are ignored (see below).

Experimental data on the energy of the corresponding electron transition for silicon-substituted nitrogen-centered radicals are still unavailable. These data, including the dependence of the value of ΔE on the Si–N–Si valence angle, can be obtained by quantum-chemical methods. The $F_3Si–\dot{N}–SiF_3$ radical was chosen as a low-molecular model of the ≡Si–N˙–Si≡ center in vitreous silica (see [19, 27] for the use of fluorine-containing low-molecular-weight compounds as the models of defects in vitreous silica). The DFT calculations at the UB3LYP/6-311G(2d,2p) level were performed. To test the efficiency of the calculation procedure, calculations were performed for H–N˙–H and F–N˙–F radicals (the C_{2v} point group of symmetry), in which the energies of the transition under consideration ($X(^2B_1) \longrightarrow A(^2A_1)$) are known to be 2 [34] and 5 eV [35], respectively. The calculations resulted in the following values for the energies of these "vertical" transitions: 2.17 eV for the H–N˙–H radical and 4.53 eV for the F–N˙–F radical (the energies of both of these states, which are characterized by different spatial sym-

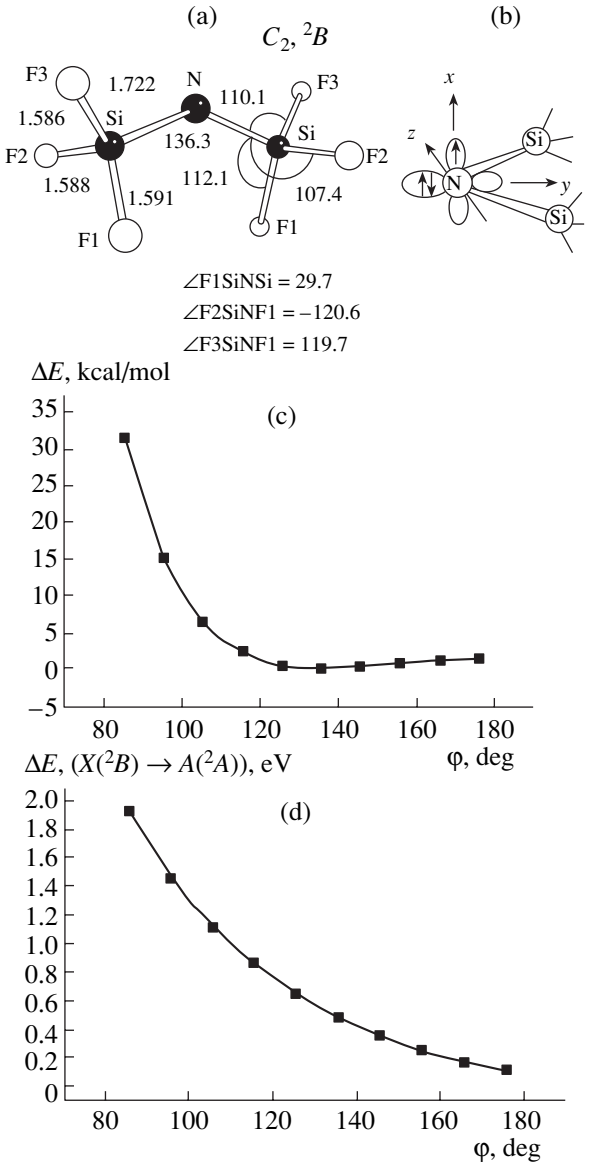

Fig. 8. $F_3Si–\dot{N}–SiF_3$ radical (the Si–N–Si valence angle was varied with the retention of its spatial symmetry C_2): (a) optimized structure; (b) schematic diagram of the electronic structure; (c) dependence of the total energy of the radical on the Si–N–Si angle; and (d) dependence of the energy of the first excited state of the radical (the energy of the vertical $^2B \longrightarrow {}^2A$ transition) on the Si–N–Si angle.

metries, were calculated by the UB3LYP/6-311G(2d,2p) method). Calculations at a higher theoretical level (QCISD(T)/6-311G(2d,2p)) gave similar values of the transition energies equal to 2.27 and 4.82 eV, respectively. Thus, the calculation results are consistent with the available experimental data. This fact suggests that, in the case of silicon-containing radicals, calculations adequately represent the energy of the optical process under discussion.

Figure 8a shows the optimized structure of the $F_3Si–N^{\cdot}–SiF_3$ radical. It exhibits the C_2 point group of symmetry. Two lower energy electronic states of the radical belong to two irreducible representations of this group of symmetry, and they are the ground $X(^2B)$ and first electronically excited $A(^2A)$ states. This provided an opportunity to calculate their energies at the same level (UB3LYP/6-311G(2d,2p)). Note that an increase in the electronegativity of substituents at the nitrogen atom is accompanied by an increase in the energy of the electron transition under discussion (ΔE): $F_3Si–^{\cdot}N–SiF_3$ (≅0.5 eV), $F_3Si–^{\cdot}N–H$ (≅1 eV, see below), $H–^{\cdot}N–H$ (≅2 eV), and $F–^{\cdot}N–F$ (≅5 eV). According to calculation data (the TD-B3LYP/6-31+G(d)//B3LYP/6-311G(2d,2p) method [26]), the energies of the excited states of $F_3Si–^{\cdot}N–SiF_3$, $F_3Si–^{\cdot}N–H$, and $H–^{\cdot}N–H$ radicals are higher than 3.95, 5.2, and 6.6 eV, respectively; thus, the use of Eq. (1) is justified.

Figure 8c demonstrates the dependence of the energy $E(\varphi)$ of the $F_3Si–^{\cdot}N–SiF_3$ radical on the Si–N–Si valence angle (φ). In these calculations, at a fixed value of this angle, all of the other geometry parameters of the radical were optimized with the retention of its symmetry (C_2).[1] As follows from the above calculation results, the total energy of the radical changed by no more than 1 kcal/mol under changes in the valence angle over the range 180°–120°; however, it rapidly increased as the valence angle was further decreased.

Figure 8d illustrates the dependence of the value of ΔE (the energy of the "vertical" transition $X(^2B) \longrightarrow A(^2A)$) on the Si–N–Si valence angle in the radical. As φ was varied over the range 90°–160°, the values of $c_1^2(2p_x(\mathrm{N}))$ and $c_2^2(2p_y(\mathrm{N}))$ (the occupancies of corresponding AOs of nitrogen in the ground and excited states of the radical) were as follows: $c_1^2(2p_x(\mathrm{N})) \cong 0.9$ and $0.70 \le c_2^2(2p_y(\mathrm{N})) \le 0.85$. Equation (1) also includes the spin–orbital coupling constant for the nitrogen atom. Assuming it to be constant and equal to 76 cm^{-1} [36] (as in the nitrogen atom in a ^2P state), according to Eq. (1), the value of $\Delta E_1 = 2.2$ eV corresponds to the lower limit of the range of $g_z = 2.008$ ($\Delta g_z = g_z - g_e \cong 0.006$), whereas $\Delta E_1 = 0.6$ eV corresponds to the upper limit $g_z = 2.024$ ($\Delta g_z \cong 0.022$).

According to calculation data (Fig. 8d), the radical in which the Si–N–Si angle is close to 90° exhibits an excitation energy of 2.2 eV. However, the energy of the system with this geometry becomes much higher (by almost 1 eV) than the equilibrium value (Fig. 8c). The Si–N–Si angle of about 125° corresponds to $\Delta E_1 =$ 0.60 eV. The range of valence angles obtained (90°–125°) seems unexpected. The ≡Si–$^{\cdot}$N–Si≡ groups, in which the Si–N–Si angle is close to 120°, are the precursors of $(\equiv Si–)_2N–Si\equiv$ radicals in vitreous silica. In the ≡Si–$^{\cdot}$N–Si≡ radical, the potential barrier of changes in the Si–N–Si angle dramatically decreased, and it would be expected that the repulsion of silicon atoms would result in a further increase in this angle.

The above estimations were made on the assumption that $\lambda(\mathrm{N}) = 76$ cm^{-1} does not depend on the Si–N–Si valence angle in the ≡Si–$^{\cdot}$N–Si≡ radical. To shift the range of valence angles for various groups of radicals to a more reasonable region (110°–150°), the constant $\lambda(\mathrm{N})$ should be decreased to 45 cm^{-1}. In the $F_3Si–^{\cdot}N–SiF_3$ radical, the nitrogen atom is bound to two silicon atoms. In this case, according to calculation data, the N atom bears a negative charge (0.7e). This can result in a decrease in the constant of spin–orbital coupling with the nitrogen atom; however, the question as to the scale of possible changes remains open.

An analogous approach was used for evaluating the value of $\lambda(\mathrm{N})$ in the NH_2 radical. In this case, available experimental data (data on the g tensor of the radical) and data on the electronic structure of the radical obtained by quantum-chemistry methods were used. The EPR spectrum of this paramagnetic center in an argon matrix was measured previously [37–39]. It was found that the radical rotates in the matrix even at helium temperatures; because of this, only the isotropic g-tensor component was found, $g_{iso} = 1/3(g_x + g_y + g_z)$. Assuming $g_x \cong 2.0023$ (the x axis is directed along the axis of the orbit of an unpaired electron) for the NH_2 radical and using Eq. (1) for g_y and g_z, we obtain

$$g_{iso} = 1/3(g_x + g_y + g_z) \cong 1/3(2.0023 + (2.0023 + 2\lambda c_1^2 c_2(1)^2/\Delta E_1) + (2.0023 + 2\lambda c_1^2 c_2(2)^2/\Delta E_2)). \quad (2)$$

The parameters of the above expression were calculated using quantum-chemistry methods: $c_1^2 = 0.98$, $c_2(1)^2 = 0.72$ and $c_2(2)^2 = 0.49$ are the occupancies of the $2p_x$, $2p_y$, and $2p_z$ AOs of nitrogen in the ground ($^2B_1$) and lower excited ($^2B_2$) and ($^2A_1$) states, respectively; $\Delta E_1 = 6.8$ eV and $\Delta E_2 = 2.14$ eV are the energies of ver-

[1] For the ≡Si–$^{\cdot}$N–Si≡ radical in vitreous silica, the relationship between the energy of the radical and the angle φ is not so unique because Si atoms are incorporated in the structure of an amorphous solid, and their properties depend on the spatial structure of their coordination sphere [32].

tical transitions to these states. The estimation was performed in the two-level approximation (it can be used when a combination of c_2^2 and ΔE is that at which one excited state mainly contributes to the change of g_i). Substituting calculated values in Eq. (2), we obtain

$$g_{iso} \cong 2.0023 + \lambda(0.6 \times 10^{-5} + 2.7 \times 10^{-5}). \quad (3)$$

This expression relates the values of g_{iso} and λ. The shift of g_{iso} from the value characteristic of a free electron (2.0023) is mainly due to g_z, which depends on ΔE_2 in accordance with Eq. (1).

However, a comparison of the calculation data with experimental results did not unambiguously answer the question as to the value of $\lambda(N)$ for the NH_2 radical. The published values of g_{iso} for the NH_2 radical differ from each other (2.0038 [37], 2.0048 [38], and 2.0058 [39]), and the reason for this difference is unknown. The above difference in the g-factor values are hardly due to stabilization conditions of the NH_2 radical; in this case, the values of ΔE_2 or $\lambda(N)$ should change by a factor of almost 2.5, which seems improbable. Assuming the constant value of $\Delta E_2 = 2.14$ eV and using Eq. (3), the value of $\lambda(N)$ was evaluated based on these data. For g_{iso} equal to 2.0038, 2.0048, and 2.0058, the values of $\lambda(N)$ are 45, 76, and 106 cm^{-1}, respectively. One of the above values (76 cm^{-1}) is equal to the value of $\lambda(N)$ given in handbooks and monographs [36].

Table 3 summarizes the experimentally determined HFC constants of an electron with magnetic nuclei in nitrogen-centered radicals ($^{\bullet}NH_2$ [39], $^{\bullet}NF_2$ [40], ≡Si–$^{\bullet}$N–H, and ≡Si–$^{\bullet}$N–Si≡ [15]) and the results of quantum-chemical calculations (the $F_3Si–^{\bullet}N–H$ and $F_3Si–^{\bullet}N–SiF_3$ radicals served as low-molecular models of ≡Si–$^{\bullet}$N–H and ≡Si–$^{\bullet}$N–Si≡ centers). In all cases, the calculations gave underestimated isotropic HFC constants for an unpaired electron with the nitrogen nucleus and adequately represented the anisotropic components of a corresponding tensor (Table 3). Note that, in the case of silicon-substituted radicals, isotropic HFC mainly contributes to the HFC constant of an unpaired electron with the ^{29}Si nucleus.

The HFC constant for an unpaired electron with the nuclei of silicon atoms in the ≡Si–$^{\bullet}$N–Si≡ radical was not measured. In the ≡Si–$^{\bullet}$N–H radical, the corresponding constant was equal to (15 ± 1) G, and the calculated values of these constants in the $F_3Si–^{\bullet}N–SiF_3$ and $F_3Si–^{\bullet}N–H$ radicals (Table 3) were similar. On this basis, it is believed that the constant in the ≡Si–$^{\bullet}$N–Si≡ radical is $a_{iso}(^{29}Si)$ = (15 ± 1) G, and the anisotropic components of the corresponding HFC tensor are no higher than 2 G.

The ≡Si–$^{\bullet}$N–Si≡ radicals in vitreous silica are different in terms of geometry (see above). Quantum-chemical calculations provide an opportunity to monitor changes in the HFC constants for an unpaired electron with nitrogen and silicon nuclei in the radical under changes in the Si–N–Si valence angle. On varying the valence angle in the $F_3Si–^{\bullet}N–SiF_3$ radical from 170° to 110°, the constant of isotopic coupling with the nitrogen or silicon nucleus changed from 7.9 to 5.7 or from 14.8 to 15.3 G, respectively. In this case, the anisotropic component of a tensor of HFC with the nitrogen atom remained almost unchanged (2b increased from 27.2 to 27.5 G). Thus, the calculated data indicate that differences in the geometry of these radicals do not result in considerable changes in the constants of the HFC of an unpaired electron with nitrogen and silicon nuclei. However, as demonstrated above, these differences strongly affect the g tensor.

2.3. (≡Si–O)$_2$(HO)Si–N$^{\bullet}$H radical. The synthesis of these radicals on the surface of silica was performed previously [17]. They were prepared from $(≡Si–O)_2Si^{\bullet}(NH_2)$ radicals by the following reactions:

$$(≡Si–O)_2Si^{\bullet}(NH_2) + N_2O \longrightarrow (≡Si–O)_2Si(NNO^{\bullet})(NH_2), \quad (III)$$

$$(≡Si–O)_2Si(NNO^{\bullet})(NH_2) \longrightarrow (≡Si–O)_2Si(O^{\bullet})(NH_2) + N_2 \longrightarrow (≡Si–O)_2Si(OH)(N^{\bullet}H) \quad (IV)$$

Paramagnetic centers formed in reaction (III) are stable at room temperature; however, they decompose with the elimination of a nitrogen molecule on heating above 373 K [10]. The resulting oxy radical abstracts an H atom from the amino group (reaction (IV)) to form the above radical centers. The EPR spectrum of this radical was measured at 77 K. At room temperature, we failed to detect the EPR signal of these paramagnetic centers. This fact suggests a considerable relaxation (reversible) broadening of the signal with temperature.

Table 2 summarizes the radiospectroscopic characteristics of the $(≡Si–O)_2Si(OH)(N^{\bullet}H)$ radical. The HFC constant for an unpaired electron with the ^{29}Si nucleus in this radical was determined with the use of a silica sample enriched in the ^{29}Si isotope. The analysis of the radiospectroscopic characteristics of the resulting paramagnetic center performed with the use of the results of quantum-chemical calculations for the model low-molecular $F_2(HO)Si–N^{\bullet}–H$ radical demonstrated that the rotation of the N–H group about the Si–N bond in this radical was unfrozen even at 77 K [17].

3. On the expected optical characteristics of ≡Si–N$^{\bullet}$–H and ≡Si–N$^{\bullet}$–Si≡ radicals. Experimental data on the optical characteristics of these radicals were not obtained. Quantum-chemical calculations demonstrated that the energy of an optical transition to a lower

excited state is only ~1 eV for ≡Si–N$^{\bullet}$–H. The energy of this transition in the ≡Si–N$^{\bullet}$–Si≡ radical is even lower. In this case, it would be expected that the difference in transition energies would lie in the range 0.3–1 eV for particular groups of radicals; this difference is due to a difference in the geometric structure (the Si–N–Si valence angle). This will result in a broadening of the optical absorption band of these centers. The oscillator strength for the transition under discussion in H–$^{\bullet}$N–H or F–$^{\bullet}$N–F radicals was calculated (the CIS/6-311G(d,p) method [26]) to be 0.0036 or 0.016, respectively. The oscillator strength for the electron transition in the $F_3Si–^{\bullet}N–SiF_3$ radical depends on the valence angle and decreased from 0.0006 to <0.0001 as the angle was increased from 85° to 175°. The oscillator strengths estimated for these transitions indicate that they are low (no higher than 10^{-3}); that is, the corresponding optical absorption bands exhibit a low intensity.

According to quantum-chemical calculation data, the relaxation of the first excited state of X–$^{\bullet}$N–Y radicals is accompanied by a change in their geometry, which mainly manifests itself in an increase in the valence angle at the nitrogen atom. This angle in H–$^{\bullet}$N–H, H–$^{\bullet}$N–F, and F–$^{\bullet}$N–F radicals increased from 102.1°, 100.1°, and 103.6° to 144.9°, 121.9°, and 120.0°, respectively. The DFT-calculated energies of vertical transitions to an excited sate (absorption) and a reverse transition from a relaxed excited state to the ground state (luminescence) for these radicals were 2.14 (0.52), 2.70 (1.91), and 4.49 (3.74) eV, respectively. According to quantum-chemical calculation results, the relaxation of an electronically excited state of the $F_3Si–N^{\bullet}$–H radical (after a vertical transition from the ground ($^2A''$) to a lower ($^2A'$) electronically excited state) is mainly accompanied by a change in the Si–N–H valence angle from 114.6° to ≈180°. In this case, the energies of the $^2A'$ and $^2A''$ states became comparable (a degenerate state). The system brought to this region of a configuration space because of approaching or intersecting electron terms will turn to the ground term but with a strongly distorted, as compared with equilibrium, geometry. As a result, the electronic excitation energy is converted into the translational energy of nuclei, which is strongly associated with the excitation of deformation vibrations of the Si–N–H group (initially, the opening of the valence angle followed by returning to its equilibrium value). Thus, the ≡Si–$^{\bullet}$N–H radical in the $^2A'$ state can undergo a radiationless transition to the ground state. As a result, it is believed that the absorption of a ~1-eV light quantum by this radical is not accompanied by luminescence. Note that this electron-excitation energy is clearly insufficient for inducing chemical transformations (degradation or isomerization) in the radical.

A similar behavior would be expected in the low-molecular $F_3Si–N^{\bullet}–SiF_3$ radical. The relaxation of a lower excited state (^2A) of this radical is also accompanied by an increase in the Si–N–Si valence angle to 180°. Consequently, the radical can return to the ground state via a radiationless transition, as in the case of $F_3Si–N^{\bullet}$–H. However, the structure relaxation of the ≡Si–N$^{\bullet}$–Si≡ radical stabilized in vitreous silica is controlled by the possibility of shifting silicon atoms as the constituents of a solid lattice. At the restricted relaxation of the geometric structure of the center, luminescence transitions (in the IR range) can also occur here. The above concepts of the optical characteristics of nitrogen-centered radicals in vitreous silica are based on model quantum-chemical calculations; however, relevant experimental data have yet to be obtained.

4.1. Reactions of ≡Si–N$^{\bullet}$–Si≡ and ≡Si–N$^{\bullet}$–H radicals with CO molecules. The stabilization of paramagnetic centers on the surface of vitreous silica provides an opportunity to study their reactivity toward various molecules from a gas phase. In this section, data on the reactivity of ≡Si–N$^{\bullet}$–Si≡ and ≡Si–N$^{\bullet}$–H radicals toward CO molecules are presented.

The course of reaction was monitored using EPR spectroscopy. Figure 9b (curve *3*) shows a fragment of the EPR spectrum of the reaction product (^{12}CO; $P_{CO} \approx 10^{-2}$ Torr; 300 K). It was obtained as the difference between the final and initial EPR signals (with consideration for the fraction of reacted paramagnetic centers, as only centers stabilized on the sample surface enter into the reaction). The central portion of the EPR spectrum of the resulting radical is not shown because of distortions due to the presence of intense absorption lines of other paramagnetic centers in this region.

The problem was solved using carbon monoxide enriched in the ^{13}C isotope (85%; $I = 1/2$) as a reagent. In this case, new lines were detected in the EPR spectrum (Fig. 9c) as a doublet (due to ^{13}C) of triplets (due to ^{14}N). In this manner, because of a high HFC constant with the ^{13}C nucleus, the EPR spectrum of the resulting radical was shifted to the regions in which it was not masked by signals from other paramagnetic centers. The distance between triplet components is consistent with the distance between the edge lines of the spectrum shown in Fig. 9b. Consequently, they are a portion of a triplet signal due to the interaction of an unpaired electron with the nitrogen nucleus in the radical.

The isotropic and anisotropic components of an HFC tensor for the ^{13}C nucleus in the resulting radical (Table 2) suggest that the major portion of spin density in this radical is localized on the 2*s* and 2*p* AOs of carbon. This is a characteristic feature of acyl-type X–C$^{\bullet}$=O radicals [41, 42]:

$$\equiv Si–N^{\bullet}–Si\equiv + CO \longrightarrow (\equiv Si–)_2N–C^{\bullet}=O$$

Dashed lines in Figs. 9b and 9c (curves *4* and *2*, respectively) illustrate the results of a simulation based on the second-order perturbation theory for the EPR spectrum of a powdered sample with the spin-Hamiltonian parameters given in Table 2 for the $(\equiv Si-)_2N-C^{\bullet}=O$ radical. The shape of an individual component was taken to be Gaussian, and the halfwidth was 2 G for the $(\equiv{}^{28}Si)_2{}^{14}N-{}^{12}C^{\bullet}=O$ radical (curve *4* in Fig. 9b) or 5 G for $(\equiv{}^{28}Si)_2{}^{14}N-{}^{13}C^{\bullet}=O$ (curve *2* in Fig. 9c). The angle between the directions of parallel *g*- and $a(^{13}C)$-tensor components in the radical was taken equal to 60° because, in acyl-type radicals ($R-{}^{13}C^{\bullet}=O$), the *g*-tensor component directed along the C=O bond exhibits a minimum value (1.9983 for the $H-C^{\bullet}=O$ radical [41]), and the $a_{\parallel}(^{13}C)$ component, according to the results of quantum-chemical calculations (see below), is directed at such an angle to it. In Figs. 9b and 9c, it can be seen that the experimental and calculated EPR spectra are consistent with one another.

Figure 9a shows the optimized structure of the model low-molecular $(F_3Si-)_2N-C^{\bullet}=O$ radical. The arrangement of Si, N, C, and O atoms in this structure is nearly planar. This geometry is favorable for the stabilization of the π system of the radical. The radical exhibits two equivalent equilibrium positions, in which the oxygen atom approaches either one or the other silicon atom. Table 4 summarizes the calculated radiospectroscopic characteristics of the radical. The constants of the HFC of an unpaired electron with silicon atoms are noticeably different; the higher constant belongs to the silicon atom that occupies the *cis* position in the Si–N–C=O unit. Note that the calculated and experimental HFC constants for ^{13}C and ^{14}N atoms in this radical are consistent with one another.

In the $(\equiv Si)_2N-C^{\bullet}=O$ radical, in which the silicon atoms are constituents of a solid, only the internal rotation of the C=O unit about the N–C bond is possible. The calculated height of a barrier for this rotation in the $(F_3Si-)_2N-C^{\bullet}=O$ radical was $E_a = 9.8$ kcal/mol. In the transition state, the C=O unit is turned through ≅90° with reference to an equilibrium position and the oxygen atom is approximately equidistant from the silicon atoms. The shape of the X-band EPR spectrum of a paramagnetic center is affected by motions at frequencies of $>10^7$ s^{-1}. At the barrier height specified above, the frequency of transitions between two equilibrium positions at 300 K is $\sim 10^{13}\exp(-E_a/RT)$ $s^{-1} \approx 10^6$ s^{-1}. However, the turn of the C=O group about the N–C bond near an equilibrium position at room temperature is as high as a few tens of degrees. This results in a partial averaging of the anisotropic *g*- and *a*-tensor components of the radical.

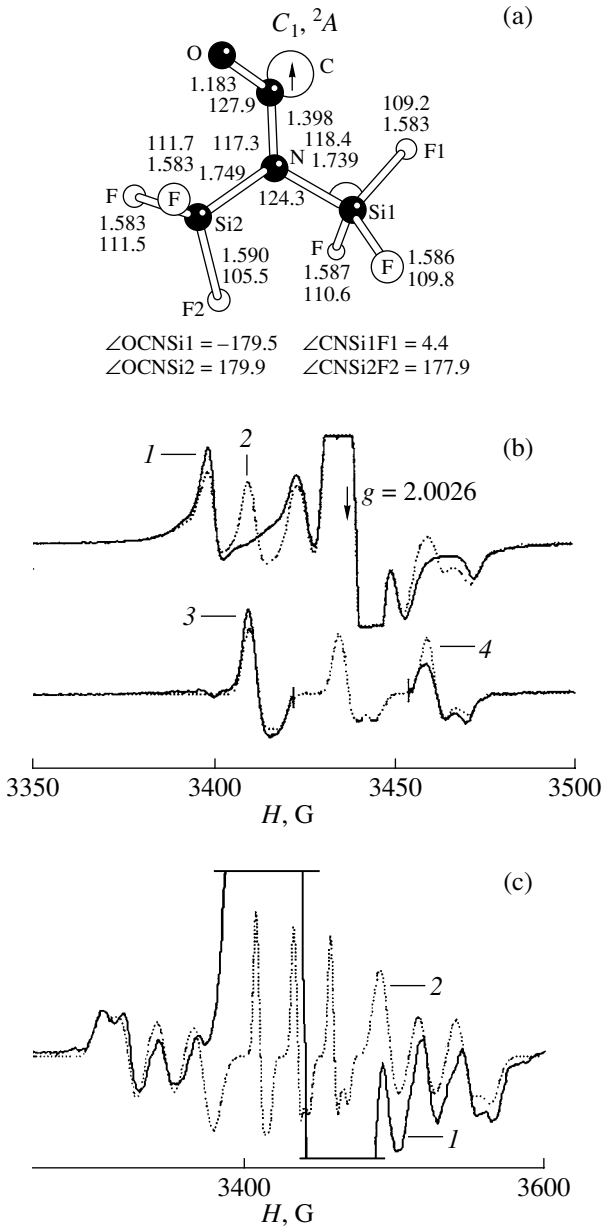

Fig. 9. Structure and EPR spectra of the reaction products of $\equiv Si-{}^{\bullet}N-Si\equiv$ radicals with CO molecules (the spectra were measured at 300 K): (a) the optimized structure of the $(F_3Si)_2N-{}^{\bullet}C=O$ radical; (b) the EPR spectra of radicals (*1*) in a mechanically activated $SiO_2(N)$ sample and (*2*) in this sample after contact with ^{12}CO molecules at 300 K, (*3*) a fragment of the EPR spectrum of the resulting $(\equiv Si-)_2N-{}^{12}C^{\bullet}=O$ radical, and (*4*) the result of a numerical simulation of the EPR spectrum of the $(\equiv Si-)_2N-{}^{12}C^{\bullet}=O$ radical (see the text); (c) (*1*) the EPR spectrum of the product of the addition of a ^{13}CO molecule to the $\equiv Si-{}^{\bullet}N-Si\equiv$ radical and (*2*) the result of a numerical simulation of the EPR spectrum of $(\equiv Si-)_2N-{}^{13}C^{\bullet}=O$ (0.9) + $(\equiv Si-)_2N-{}^{12}C^{\bullet}=O$ (0.1) radicals (three central lines in the spectrum belong to the latter radical) (see the text).

Table 4. Calculated HFC constants for the radicals $F_2(HO)Si–HN–C^{\cdot}=O$ (*A*, *cis* configuration of Si, N, C, and O atoms), $F_2(HO)Si–HN–C^{\cdot}=O$ (*B*, *trans* configuration of Si, N, C, and O atoms), and $(F_3Si)_2N–C^{\cdot}=O$(*C*)*

Radical	Atom					
	^{13}C	^{14}N	$^{1}H(N)$	$^{29}Si_2$**	$^{29}Si_1$	$^{1}H(O)$
A	175.8	20.7	3.3	–	–31.6	–0.8
	(–17.3; –15.2; 32.5)	(–2.1; –1.4; 3.5)	(–4.0; –2.6; 6.6)		(1.5; 1.3; –2.8)	(–2.3; –0.7; 3.0)
B	162.5	32.5	28.1	–	3.1	–0.1
	(–16.2; –14.7; 31.0)	(–1.6; –1.3; 2.9)	(–2.7; –0.8; 3.5)		(0.2; 0.2; –0.4)	(–0.5; –0.4; 0.9)
C	191.2	28.3	–	3.0	–30.0	–
	(–16.9; –14.5; 31.4)	(–2.0; –1.6; 3.6)		(0.4; 0.3; –0.7)	(1.4; 1.3; –2.7)	

Note: DFT calculation (UB3LYP/6-311G(d,p)); the constants are in gausses. The first row shows the values of isotropic components, and the next row (in parentheses) shows the principal values of the tensor of anisotropic HFC of the unpaired electron with the corresponding nucleus.

* The optimized structures of radicals *A* and *B* were published elsewhere [17], and the optimized structure of radical *C* is shown in Fig. 9a.

** This constant belongs to the silicon atom that occupies the *trans* position in the O, C, N, and Si fragment of radical *C* (Fig. 9a).

The $(\equiv Si–O–)_2(HO)Si–HN^{\cdot}$ radicals also react with CO molecules [17]:

$$(\equiv Si–O–)_2(HO)Si–HN^{\cdot} + CO \longrightarrow (\equiv Si–O–)_2(HO)Si–HN–C^{\cdot}=O$$

This reaction can be performed at 77 K. Table 2 summarizes the radiospectroscopic characteristics of the resulting radical. The heating of a sample to 300 K irreversibly changed the shape of the EPR spectrum of paramagnetic centers. However, the concentration of these centers remained unchanged (to within 20%) in this case. The conversion occurred over the temperature range 160–190 K.

An analysis of the experimental data using the results of quantum-chemical calculations demonstrated that the two radicals are chemically identical ($>$(HO)Si–HN–$C^{\cdot}$=O) but conformationally different [17]. The addition of the CO molecule to the $\equiv Si–N^{\cdot}–H$ radical at low temperatures was accompanied by the formation of ≡Si–HN–$C^{\cdot}$=O in a *trans* configuration. The latter is partially converted into a more stable *cis* form on heating. This process is detected by EPR spectroscopy as a transformation of radicals. The ≡Si–HN–$C^{\cdot}$=O(*cis*) $\rightleftharpoons$ ≡Si–HN–$C^{\cdot}$=O(*trans*) equilibrium is established between the two radical species. The experimental equilibrium constant determined at 300 K is 0.25 ± 0.1. If the observed effect is related to differences in the heats of formation of the radicals, the *cis* form is more stable than the *trans* form by ~1 kcal/mol (this is consistent with the results of quantum-chemical calculations (see below)).

The *cis* form of the radical has a lower energy because of the formation of an intramolecular hydrogen bond between the hydrogen atom of the hydroxyl group and the oxygen atom of the O=C group ($\angle HOSiN = 0°$; $r(H\cdots O) = 0.207$ nm). According to the results of quantum-chemical calculations, the heat of formation of this conformer is lower than that of the most stable species of *trans* structures by 1.5 kcal/mol.

As estimated from experimental data, the activation energy of the *trans–cis* conversion is 12.7 ± 0.5 kcal/mol [17]. This transition results from the turn of the C=O group about the N–C bond. The activation energy of rearrangement for the low-molecular $F_3Si–HN–C^{\cdot}=O$ radical was calculated to be 13.2 kcal/mol, which is consistent with the experimentally estimated value.

4.2. Thermal stability of $(\equiv Si–)_2N–C^{\cdot}=O$ and ≡Si–HN–$C^{\cdot}$=O radicals. The above radicals are stable at room temperature. They begin to decay as the temperature is increased to 373 K. The course of this process was monitored by EPR spectroscopy. A decrease in the concentration of radicals was accompanied by the elimination of a CO molecule. Moreover, in the case of ≡Si–HN–$C^{\cdot}$=O, a parallel reaction path of its conversion was found, namely, the degradation with the elimination of an H atom [17]

$$(\equiv Si)_2N–C^{\cdot}=O, \quad \equiv Si–HN–C^{\cdot}=O \longrightarrow (\equiv Si)_2N^{\cdot}, \quad \equiv Si–N^{\cdot}H + CO;$$

$$\equiv Si–HN–C^{\cdot}=O \longrightarrow \equiv Si–N=C=O + H^{\cdot}$$

Based on the kinetic data, the activation energy of the unimolecular degradation of acyl radicals was estimated at (29.5 ± 1) kcal/mol (the preexponential factor was taken equal to 10^{13} s^{-1}). Because the activation energy of the addition of the CO molecule to nitrogen-centered radicals is no higher than 2 kcal/mol (the reaction occurs at low pressures of CO at 77 K), the heat effect of the elimination of the CO molecule is 27–30 kcal/mol.

5. Reactions of $\equiv Si–N^{\cdot}–H$ and $\equiv Si–N^{\cdot}–Si\equiv$ radicals with H_2. Molecular hydrogen is one of the few compounds that can be introduced into the bulk of vit-

reous silica. Chemical processes with the participation of molecular hydrogen are used for modifying the structure of this widely used material. The defects of vitreous silica play an important role in these processes.

The exposure of ≡Si–N$^{\bullet}$–H radicals to an atmosphere of H_2 at room temperature is accompanied by the chemisorption of the gas in an amount that is comparable with the number of radicals and by the disappearance of the EPR spectrum of these radicals (radiospectroscopic measurements were performed at 77 K (see Section 1.1.)). When diamagnetic centers of the silylene type ((≡Si–O)$_2$Si:) also occurred on the sample surface in addition to the paramagnetic ≡Si–N$^{\bullet}$–H centers, the decay of radicals in an atmosphere of H_2 was accompanied by the quantitative formation of new paramagnetic centers: ≡Si$^{\bullet}$–H. The appearance of the ≡Si$^{\bullet}$–H radicals in the system suggests that H atoms are formed in the course of the reaction of ≡Si–N$^{\bullet}$–H radicals with H_2 molecules. The H atoms add to silylene groups, which are effective free-radical scavengers [23, 27]. The above experimental data demonstrate that the process under consideration occurs in accordance with the following reaction scheme:

$$\equiv Si{-}N^{\bullet}{-}H + H_2(D_2) \longrightarrow \equiv Si{-}NH_2(HD) + H(D)^{\bullet};$$

$$H(D)^{\bullet} + (\equiv Si{-}O)_2Si: \longrightarrow (\equiv Si{-}O)_2Si^{\bullet}{-}H(D)$$

The reaction of ≡Si–N$^{\bullet}$–H radicals with deuterium molecules occurs in a similar manner. The rates of both processes are proportional to gas pressure over the sample, and the rate constants of these bimolecular reactions at 301 K are $k(H_2) = (2.7 \pm 0.3) \times 10^{-17}$ cm^3 molecule^{-1} s^{-1} and $k(D_2) = (5.1 \pm 0.5) \times 10^{-18}$ cm^3 molecule^{-1} s^{-1} [17]. Thus, the value of the isotope effect of this reaction at room temperature is close to 5.

In reactions with the participation of H atoms, both classical (overbarrier) and quantum (underbarrier, tunneling) modes of overcoming an activation barrier are possible. The value of the isotope effect suggests that the reaction occurs via a classical (overbarrier) path at room temperature. Assuming a normal value of the preexponential factor (10^{-11} cm^3 molecule^{-1} s^{-1}) for the activation energy of this reaction, we obtain E = 7.7 (8.7) kcal/mol (processes with the participation of H_2 (D_2) molecules).

Figure 10a shows the optimized structure of the transition state for the reaction of H abstraction from the hydrogen molecule by the $F_3Si–N^{\bullet}–H$ radical as a low-molecular model of the ≡Si–N$^{\bullet}$–H surface center. The results of calculations of the activation energy and heat effect of this reaction (the former and latter (in parentheses) figures indicate the results of calculations at the DFT level and at the G2MP2 level (Table 3), respectively) and analogous characteristics for the $H_2N^{\bullet}$ reaction (published data [44] are available for the latter reaction) are given below:

$$F_3Si{-}N^{\bullet}{-}H + H_2 \longrightarrow TS + 5.7\ (10.4)\ \text{kcal/mol}$$

$$\longrightarrow F_3Si{-}NH_2 + H^{\bullet} - 8.3\ (-11.8)\ \text{kcal/mol},$$

$$H{-}N^{\bullet}{-}H + H_2 \longrightarrow TS + 7.1\ (13.5)\ \text{kcal/mol}$$

$$\longrightarrow NH_3 + H^{\bullet} + 1.1(-2.3)\ \text{kcal/mol}.$$

According to Hack *et al.* [43], the activation energy of the latter reaction is ~9 kcal/mol, and its heat effect (at 298 K) is –4 kcal/mol [44]. As would be expected, calculations at the G2MP2 level better reproduced the heat effects of reaction. In general, the results of calculations are consistent with the experimental data, and they suggest that the reactivity of the $F_3Si–N^{\bullet}–H$ silicon-containing radical in this reaction is higher than that of H–N$^{\bullet}$–H. This manifests itself in both a decrease in the activation energy of the reaction and an increase in its heat effect.

The ≡Si–N$^{\bullet}$–Si≡ radicals that were stabilized on the surface of mechanically activated SiO_2(N) silica also reacted with H_2 molecules. The process was accompanied by the chemisorption of the gas in an amount that was comparable to the number of reacted radicals (recall that a portion of these radicals was stabilized in near-surface layers of the material, and they were inaccessible to molecules from a gas-phase). The (≡Si–O)$_2$Si diamagnetic centers also occurred on the surface of the test sample, and the decay of radicals in an atmosphere of H_2 was accompanied by the formation of new paramagnetic centers: ≡Si–H radicals. Thus, in this case, as well as in the reaction of ≡Si–N$^{\bullet}$–H radicals with H_2 molecules, the process occurred as follows:

$$\equiv Si{-}N^{\bullet}{-}Si\equiv + H_2 \longrightarrow \equiv Si{-}NH{-}Si\equiv + H^{\bullet};$$

$$H^{\bullet} + (\equiv Si{-}O)_2Si: \longrightarrow (\equiv Si{-}O)_2Si^{\bullet}{-}H$$

Figure 10c demonstrates the kinetic curve of decay of ≡Si–N$^{\bullet}$–Si≡ radicals in this process at 301 K, as measured from a decrease in the number of H_2 molecules in a gas phase. However, in this case, unlike the reaction with the participation of ≡Si–N$^{\bullet}$–H radicals, the rate of bimolecular reaction decreased in the course of the process rather than obeyed the rate law $dN/dt = kP_{H_2}(t)N$. Therefore, the kinetic curve of radical decay was plotted in the $N/N_0 - \ln[\int P_{H_2}(t)dt]$ coordinates (here, N_0 and N are the initial and current concentrations of ≡Si–N$^{\bullet}$–Si≡ radicals, respectively, and $\int P_{H_2}(t)dt$ is the exposure: a quantity proportional to the number of collisions of gas molecules with a surface center in the time t). The kinetic curve was adequately linearized in these coordinates. The kinetic behavior observed suggests that particular fractions of radicals

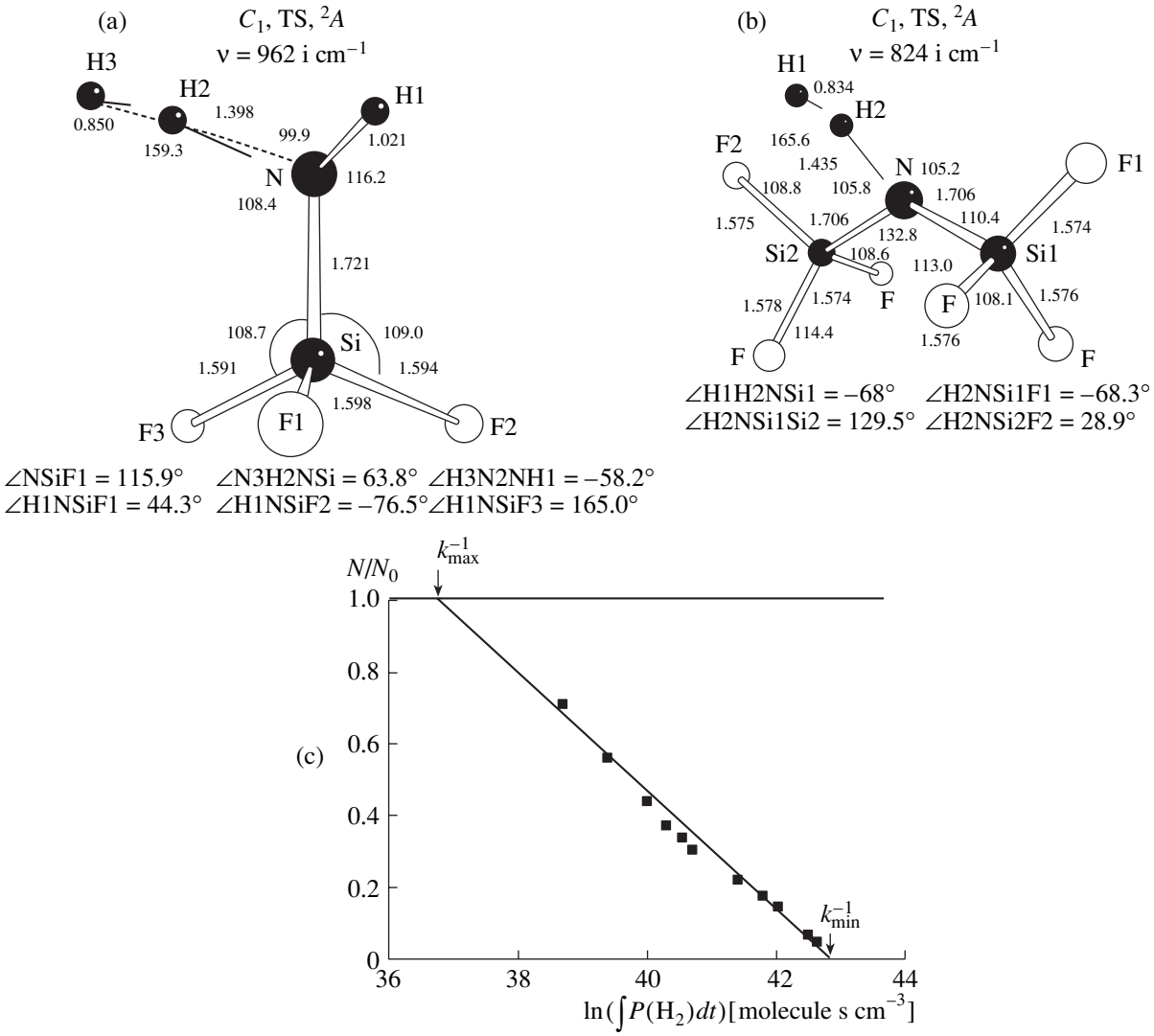

Fig. 10. Reactions of the nitrogen-centered radicals ≡Si–$^{\bullet}$N–H and ≡Si–$^{\bullet}$N–Si≡ with molecular hydrogen: (a) the structure of the transition state for the reaction $F_3Si–^{\bullet}N–H + H_2 \longrightarrow F_3Si–NH_2 + H^{\bullet}$; (b) the structure of the transition state for the reaction $F_3Si–^{\bullet}N–SiF_3 + H_2 \longrightarrow F_3Si–NH–SiF_3 + H^{\bullet}$ (for both of the transition states, characteristic imaginary frequencies are given and atomic shifts that take place when moving along the reaction coordinate are shown); and (c) kinetic curve of the decay of ≡Si–$^{\bullet}$N–Si≡ radicals in the course of the reaction ≡Si–$^{\bullet}$N–Si≡ + $H_2 \longrightarrow$ ≡Si–NH–Si≡ + $H^{\bullet}$ at 301 K (for comments, see the text).

differ in their reactivity toward hydrogen, and the distribution function of the number of radicals that react with the rate constant k is $n(k) \sim 1/k$ ($k_{min} \le k \le k_{max}$) [22]. Extrapolating the linear portion to intersect the axes at $N/N_0 = 0$ and 1, we estimated the values of k_{min} and k_{max}, which characterize the distribution [22]. They were found to be equal to 2.5×10^{-19} and 1.1×10^{-16} cm^3 molecule^{-1} s^{-1}, respectively.

This result might have been expected. It is believed that the observed kinetic nonequivalence of radical centers is due to structural differences (see Section 2.3.). A comparison of the range of rate constants k for the reaction of ≡Si–N$^{\bullet}$–Si≡ radicals with the rate constant of the reaction with the participation of ≡Si–N$^{\bullet}$–H $k(H_2) = (2.7 \pm 0.3) \times 10^{-17}$ cm^3 molecule^{-1} s^{-1} demonstrates that one portion of ≡Si–N$^{\bullet}$–Si≡ radicals exhibits a higher reactivity, whereas the other portion exhibits a lower reactivity in this process. Assuming that the preexponential factor for the bimolecular reaction under consideration has a typical value of 10^{-11} cm^3 molecule^{-1} s^{-1}, we obtain the following activation energies: $E_{max} = 10.5$, $E_{min} = 6.9$, and $E = 7.7$ kcal/mol (E_{min} and E_{max} are the activation energies of reactions that occur with the rate constants k_{max} and k_{min}, respectively).

Figure 10b shows the structure of the transition state for the reaction $F_3Si–N^{\bullet}–SiF_3 + H_2 \longrightarrow F_3Si–NH–SiF_3 + H^{\bullet}$ (calculated at the UB3LYP/6-311G(2d,2p) level).

According to calculation data, the activation energy (4.8 kcal/mol) and the heat effect (–11 kcal/mol) of this reaction are lower by 1 kcal/mol and higher by 2.7 kcal/mol, respectively, than those of the reaction $F_3Si–N^{\bullet}–H + H_2 \longrightarrow F_3Si–NH_2 + H^{\bullet}$. Thus, the $\equiv Si–N^{\bullet}–Si\equiv$ radicals in a free state exhibit a higher reactivity. The higher heat effect of the reaction of H abstraction with the participation of these radicals is indirect evidence for the above conclusion.

6. On the strengths of Si–O and Si–N bonds in vitreous silica. The O atom and the NH group are isoelectronic; this implies a certain similarity between their physicochemical characteristics. In nitrogen-doped vitreous silicas, the $\equiv Si–O^{\bullet}$ and $\equiv Si–N^{\bullet}–H$ ($\equiv Si–N^{\bullet}–Si\equiv$) paramagnetic centers can be stabilized, in which an unpaired electron is localized on an electronegative atom (oxygen or nitrogen). Which of these states is thermodynamically more stable? We calculated the enthalpies $\Delta H(0\ K)$ (kcal/mol) of reactions with the participation of fluorine-substituted compounds, which simulated groups in vitreous silica:

$$F_3Si–O–SiF_3 + {}^{\bullet}NH–SiF_3 \longrightarrow F_3Si–NH–SiF_3 \longrightarrow + {}^{\bullet}O–SiF_3 + 20.7(22.3), \quad (V)$$

$$F_3Si–O–SiF_3 + F_2Si–{}^{\bullet}N–SiF_3 \longrightarrow F_3Si–N(SiF_3)_2 + {}^{\bullet}O–SiF_3 + 21.5. \quad (VI)$$

The calculations for reaction (V) were performed at the UB3LYP/6-311G(d,p) and G2(MP2//UB3LYP/6-311G(d,p)) (figures in parentheses) levels. From the results, it follows that both of the methods give similar heat effects of this reaction (the latter system, which is bulkier, was calculated using only the former method). Thus, in this system, the stabilization of a nitrogen-centered paramagnetic center is thermochemically favorable (by almost 20 kcal/mol). As a result, the equilibrium $\equiv Si–N^{\bullet}–Si\equiv + \equiv Si–O–Si \rightleftharpoons \equiv Si–N(Si\equiv)_2 + {}^{\bullet}O–Si\equiv$ in nitrogen-doped vitreous silica is shifted to the left (if external conditions permit the establishment of a thermodynamic equilibrium).

The heat effects of reactions (V) and (VI) are due to differences in the strengths of Si–O and Si–N bonds in vitreous silica. Consequently, the bond of silicon with oxygen is stronger than that with nitrogen by almost 20 kcal/mol. The results of direct calculations of the strengths of Si–O and Si–N bonds ($\Delta H(0\ K)$, kcal/mol) in the molecules of $F_3Si–O–SiF_3$, $F_3Si–NH–SiF_3$, and $F_3Si–N(–SiF_3)_2$ are given below (the former and latter (in parentheses) figures refer to the results of calculations at the UB3LYP/6-311G(d,p) and G2(MP2//UB3LYP/6-311G(d,p) levels, respectively):

$$F_3Si–O–SiF_3 \longrightarrow F_3Si^{\bullet} + {}^{\bullet}O–SiF_3 + 139.7(152.6);$$

$$F_3Si–NH–SiF_3 \longrightarrow F_3Si^{\bullet} + {}^{\bullet}NH–SiF_3 + 119.0(129.1);$$

$$F_3Si–N(–SiF_3)_2 \longrightarrow F_3Si^{\bullet} + {}^{\bullet}N(–SiF_3)_2 + 118.2.$$

Based on the data obtained, the strengths of Si–O and Si–N bonds in vitreous silica can be estimated at 150 ± 5 and 130 ± 5 kcal/mol, respectively.

Various siloxane bond strengths in vitreous silica have been given in the literature. Silin with coauthors [45, 46] reported on a value of 88 kcal/mol, whereas Araujo [47] cited a value of 111 kcal/mol (with no reference to the origin). These are estimated values based on a number of assumptions. Pacchioni and Ierano [48] calculated the strength of the Si–O bond by quantum-chemical methods using a low-molecular cluster containing a siloxane bond (the $Si_2O_7H_6$ molecule calculated at the MP2//HF level) and obtained a value of 126.8 kcal/mol. The value obtained in this work is noticeably higher. In the cited publication, the average strength of the Si–O bond is given, which is equal to a half of the enthalpy of cleavage of two Si–O bonds (in the molecule and the resulting oxy radical): $\equiv Si–O–Si\equiv \longrightarrow \equiv Si^{\bullet} + {}^{\bullet}O–Si\equiv \longrightarrow \equiv Si^{\bullet} + O(^3P) + {}^{\bullet}Si\equiv$. However, the strength of the Si–O bond in glass (the former reaction) is noticeably higher than that in the oxy radical. Moreover, the calculations [48] were performed at another theoretical level.

ACKNOWLEDGMENTS

The author is grateful to the following staff members of the Fiber Optics Research Center, General Physics Institute, Russian Academy of Sciences: K.M. Golant, who initiated this study; V.V. Khrapko for the preparation of $SiO_2(N)$ samples; and V.M. Mashinskii and A.L. Tomashuk for the irradiation of these samples. L.S. Gulyaeva, E.A. Markevich, and E.P. Permenova also took part in this study. This work was supported by the Russian Foundation for Basic Research (RFBR) (project no. 03-03-32712a) and the Russian Academy of Sciences (OKhNM program "Theoretical and Experimental Studies on the Nature of the Chemical Bond and the Mechanisms of the Most Important Chemical Reactions and Processes"). Calculations were performed using the GAUSSIAN-94 [26] at the Zelinskii Institute of Organic Chemistry, Russian Academy of Sciences, within the framework of RFBR project no. 98-07-90290.

REFERENCES

1. Habraken, F.H.P.M. and Kuiper, A.E.T., *Mater. Sci. Eng., R*, 1994, vol. 12, p. 123.
2. Ellis, K.A. and Buhrman, R.A., *IBM J. Res. Dev.*, 1999, vol. 43, p. 287.
3. Gusev, E.P., Lu, H.C., Garfunkel, E., Gustafsson, T., and Green, M., *IBM J. Res. Dev.*, 1999, vol. 43, p. 265.
4. Worhoff, K., Lambeck, P.V., and Driessen, A., *J. Lightwave Technol.*, vol. 17, no. 8, p. 1401.

5. Dianov, E.M., Golant, K.M., Khrapko, R.R., Kurkov, A.S., Leconte, B., Douay, M., and Niay, P., *Electron. Lett.*, 1997, vol. 33, no. 3, p. 236.
6. Dianov, E.M., Golant, K.M., Khrapko R.R., and Tomashuk, A.L, *Electron. Lett.*, 1995, vol. 31, no. 17, p. 1490.
7. Dianov, E.M., Golant, K.M., Khrapko, R.R., Medvedkov, O.I., Tomashuk, A.L., and Vasil'ev, S.A., *Opt. Mater.*, 1996, vol. 5, p. 169.
8. Weeks, R.A., *J. Non-Cryst. Solids*, 1994, vol. 179, p. 1.
9. Radtsig, V.A. and Bystrikov, A.V., *Kinet. Katal.*, 1978, vol. 19, p. 713.
10. Radtsig, V.A., *Kinet. Katal.*, 2001, vol. 42, no. 5, p. 696.
11. Hirao, T., Setsune, K., Kitagawa, M., Kamada, T., Ohmura, T., Wasa, K., and Izumi, T., *Jpn. J. Appl. Phys.*, 1988, vol. 27, p. L21.
12. Kubler, L., Haug, R., Ringeisen, F., and Jaegle, A., *J. Non-Cryst. Solids*, 1983, vol. 54, p. 27.
13. Tsai, T.E., Griscom, D.L., and Friebele, E.J., *Phys. Rev.*, 1988, vol. 38, no. 3, p. 2140.
14. Yount, J.T., Kraus, G.T., Lenahan, P.M., and Krick, D.T., *J. Appl. Phys.*, 1991, vol. 70, no. 9, p. 4969.
15. Mackey, J.H., Boss, J.W., and Kopp, M., *Phys. Chem. Glasses*, 1970, vol. 11, no. 6, p. 205.
16. Friebele, E.J., Griscom, D.L., and Hickmott, T.W., *J. Non-Cryst. Solids*, 1985, vol. 71, p. 351.
17. Radtsig, V.A., *Kinet. Katal.*, 2002, vol. 43, no. 6, p. 862.
18. Radtsig, V.A. and Kozlov, S.N., *Kinet. Katal.*, 2001, vol. 42, no. 1, p. 62.
19. Radtsig, V.A., *Kinet. Katal.*, 1996, vol. 37, no. 2, p. 310.
20. Pavy, D., Moisan, M., Saada, S., Chollet, P., Leprince, P., and Marrec, J., *Proc. 12th Eur. Conf. on Optical Communications*, Barcelona, 1986, p.19.
21. Dianov, E.M., Golant, K.M., Khrapko, R.R., Kurkov, A.S., and Tomashuk, A.L., *J. Lightwave Technol.*, 1995, vol. 13, no. 7, p. 1471.
22. Radtsig, V.A., *Kinet. Katal.*, 1979, vol. 20, no. 5, p. 1206.
23. Radzig, V.A., *Colloids Surf., A*, 1993, vol. 74, p. 91.
24. Morterra, C. and Low, M.J.D., *J. Chem. Soc., Chem. Commun.*, 1968, p. 203.
25. Morterra, C. and Low, M.J.D., *Ann. N. Y. Acad. Sci.*, 1972, vol. 220, p. 135.
26. *Gaussian-94, Revision D.1*, Frisch, M. J., Trucks, G.W., Schlegel, H.B., Gill, P.M.W., Johnson, B.G., Robb, M.A., Cheeseman, J.R., Keith, T., Petersson, G.A., Montgomery, J.A., Raghavachari, K., Al-Laham, M.A., Zakrzewski, V.G., Ortiz, J.V., Foresman, J.B., Cioslowski, J., Stefanov, B.B., Nanayakkara, A., Challacombe, M., Peng, C.Y., Ayala, P.Y., Chen, W., Wong, M.W., Andres, J.L., Replogle, E.S., Gomperts, R., Martin, R.L., Fox, D.J., Binkley, J.S., Defrees, D.J., Baker, J., Stewart, J.P., Head-Gordon, M., Gonzalez, C., and Pople, J.A., Eds., Pittsburgh: Gaussian Inc., 1995.
27. Radtsig, V.A., *Chem. Phys. Rep.*, 2001, vol. 19, no. 3, p. 469.
28. Becke, A.D., *J. Chem. Phys.*, 1993, vol. 98, p. 5648.
29. Lee, C., Yang, W., and Parr, R.G., *Phys. Rev. B: Condens. Matter*, 1988, vol. 37, p. 785.
30. Curtiss, L.A., Raghavachari, K., and Pople, J.A., *J. Chem. Phys.*, 1993, vol. 98, no. 2, p. 1293.
31. El'yashevich, M.A., *Atomnaya i molekulyarnaya spektroskopiya* (Atomic and Molecular Spectroscopy), Moscow: Fizmatgiz, 1962.
32. Radzig, V.A., *Defects in SiO_2 and Related Dielectrics: Science and Technology*, Pacchioni, G., Skuja, L., and Griscom, D.L., Eds., Dordrecht: Kluwer, 2000, p. 339.
33. Kanzig, W. and Cohen, M.H., *Phys. Rev. Lett.*, 1959, vol. 3, p. 509.
34. Dressler, K. and Ramsay, D.A., *Philos. Trans. R. Soc.*, 1959, vol. A251, no. 1002, p. 553.
35. Jacox, M.E., Milligan, D.E., Guillory, W.A., and Smith, J.J., *J. Mol. Spectrosc.*, 1974, vol. 52, p. 322.
36. Atkins, P.W. and Symons, M.C.R., *The Structure of Inorganic Radicals*, Amsterdam: Elsevier, 1967.
37. Cochran, E.L., Adrian, F.J., and Bowers, V.A., *J. Chem. Phys.*, 1969, vol. 51, p. 2759.
38. Fischer, P.H., Charles, S.W., and McDowell, C.A., *J. Chem. Phys.*, 1967, vol. 46, p. 2162.
39. Misochko, E.Ya., Goldschleger, I.U., and Akimov, A.V., *Fiz. Nizk. Temp.*, 2000, vol. 26, no. 9/10, p. 981.
40. Kasai, P.H. and Whipple, E.B., *Mol. Phys.*, 1965, vol. 9, p. 497.
41. Adrian, F.J., Cochran, E.L., and Bowers, V.A., *J. Chem. Phys.*, 1962, vol. 36, p. 1661.
42. Holmerg, R.W., *J. Chem. Phys.*, 1969, vol. 51, p. 3255.
43. Hack, W., Rouveirolles, P., and Wagner, H.G., *J. Phys. Chem.*, 1986, vol. 90, p. 2505.
44. Lias, S.G., Liebman, J.F., Levin, R.D., and Kafafi, S.A., *NIST Standard Reference Database 25: Structure and Properties*, 1994.
45. Silin', A.R. and Trukhin, A.I., *Fizika tverdogo sostoyaniya: tochechnye defekty i elementarnye vozbuzhdeniya v kristallicheskom i stekloobraznom SiO_2* (Solid-State Physics: Point Defects and Elementary Excitations in Crystalline and Vitreous SiO_2), Riga: Zinatne, 1985.
46. Silin, A.R. and Lace, L.A., *J Non-Cryst. Solids*, 1992, vol. 149, p. 54.
47. Araujo, R., *J. Non-Cryst. Solids*, 1996, vol. 197, p. 164.
48. Pacchioni, G. and Ierano, G., *Phys. Rev. B: Condens. Matter*, 1997, vol. 56, p. 7304.